JGR Planets

RESEARCH ARTICLE
10.1029/2023JE007816

Slopes of Lunar Crater Size-Frequency Distributions at Copernican-Aged Craters

A. Oetting[1], N. Schmedemann[1], H. Hiesinger[1], and C. H. van der Bogert[1]

[1]Institut für Planetologie, Universität Münster, Münster, Germany

Key Points:

- We studied small craters on young ejecta blankets to evaluate if the lunar production function (PF) is viable for craters ≤10 m
- The crater size-frequency distributions (CSFDs) indicate that the PF can indeed be extended to crater diameters ≤10 m
- Our observed slopes of CSFDs at the studied Copernican-aged craters are consistent with previous findings

Correspondence to:
A. Oetting,
aoetting@uni-muenster.de

Citation:
Oetting, A., Schmedemann, N., Hiesinger, H., & van der Bogert, C. H. (2023). Slopes of lunar crater size-frequency distributions at Copernican-aged craters. *Journal of Geophysical Research: Planets*, *128*, e2023JE007816. https://doi.org/10.1029/2023JE007816

Received 3 APR 2023
Accepted 26 SEP 2023

Abstract Craters on the lunar surface can provide valuable information about the timing and sequence of surface-forming processes on the Moon. A commonly used method for age determination is the analysis of the crater size-frequency distribution (CSFD) to which a production function (PF) is fitted that represents the size-frequency distribution of the impactors. However, the commonly used PF of Neukum (1983) is valid for crater diameters between 10 m and 300 km. Neukum et al. (2001, https://doi.org/10.1007/978-94-017-1035-0_3) revised the PF for crater diameters of 100 m–200 km. However, it is suggested to also be valid for the diameter range of 10 m–300 km as well. To assess whether we can extend a PF to craters ≤10 m in diameter, we investigated the slopes of the CSFDs of small craters formed on ejecta of young Copernican-aged craters Giordano Bruno, Moore F, North Ray, and South Ray. A PF for smaller diameters would allow dating of young geological units, which are typically small, and would reduce the statistical error in age determinations, since smaller craters are more abundant. However, small craters are strongly influenced by geological factors, such as target properties, crater degradation, and secondary craters. For craters between 10 and 20 m we obtain a steeper CSFD slope than Neukum's proposed −3 slope (cumulative), whereas for craters ≤10 m the slope is about −3. We conclude that the PF of Neukum (1983) provides a reasonable CSFD slope for smaller craters, although it was not developed for this crater diameter range.

Plain Language Summary Since the formation of the Moon, impactors have randomly hit the lunar surface. Older areas have larger and more abundant craters compared to younger areas. This relationship allows the determination of relative ages for different surfaces. A mathematical function can be fitted to the number and size of craters. This function has a specific shape and can be used to date a surface. Frequently used functions are valid between crater diameters of 10 m and 300 km. Dating young geological units is only possible if the observed craters are ≥10 m in diameter. Therefore, an extension of these functions to crater diameters ≤10 m would be beneficial. However, small craters are strongly influenced by geological factors, such as target properties, crater degradation, and secondary craters. We consider these influences in our investigation. To compare our results with previous findings, we look more closely at the slope of the function that results from the number and size of the craters. Generally, we find that one function fits well for craters ≤10 m, even though it was not designed for this diameter range. This allows a more robust age determination because small craters are more abundant, reducing the statistical error.

1. Introduction

The dating of geologic surfaces on the Moon is crucial for understanding its geologic history and evolution. Crater size-frequency distribution (CSFD) measurements are often used for determining both relative and absolute ages of surfaces, where older surfaces exhibit more and larger craters than younger surfaces (Baldwin, 1971; Neukum, 1983; Öpik, 1960; Shoemaker et al., 1970). Hence, it is assumed that the number of impact craters is directly related to time (Baldwin, 1964; Neukum, 1983; Öpik, 1960). The determination of surface ages requires the construction of a production function (PF), which indicates how many craters of a given diameter formed on an undisturbed surface of a given age (Baldwin, 1964; Neukum, 1983; Öpik, 1960). One frequently used PF was empirically derived by measuring craters on reference surfaces using Apollo era data (Neukum, 1983) and was revised in 2001 (Neukum et al., 2001).

The lunar PFs of Neukum are polynomials of 11th degree and are fitted to the measured CSFD of a given reference area to determine its crater density at an arbitrarily selected reference crater diameter, often 1 or 10 km (e.g., Hartmann & Neukum, 2001; Ivanov & Hartmann, 2007; Neukum, 1983; Neukum et al., 2001), yielding the cumulative number (N) of craters ≥1 or 10 km, that is, $N(1)$ or $N(10)$. Hence, the $N(1)$ or $N(10)$ provide relative

ages. Another PF was developed by Hartmann (1999), who fitted three power laws to different diameter ranges (>64, 1.41 to <64, and 0.3–1.41 km) of the CSFDs.

Crater densities at chosen reference diameters can be correlated with absolute radiometric and exposure ages of lunar rock and soil samples returned from lunar sites, which allows the construction of a chronology function (e.g., Neukum, 1983; Neukum et al., 2001; Robbins, 2014), which can be used to determine absolute model ages (AMAs) and can, in principle, be applied to any area on the lunar surface. Thus, with these two functions, it is possible to derive relative ages and AMAs for the lunar surface. A limitation, however, is that the PF is only valid for crater diameters of 10 m–300 km (Neukum, 1983). The PF of Neukum et al. (2001) was refined in crater diameters between 100 m and 200 km, but it is also suggested to be valid for the crater diameter range between 10 m and 300 km (Ivanov et al., 2001). The power laws of Hartmann (1999) are valid in the crater diameter range between 0.3 and >64 km. With the increased image resolution of more recent missions (Haruyama et al., 2008; Robinson, 2011), it has been possible to perform CSFD measurements for crater diameters down to a few meters. Thus, it would be beneficial to be able to extend available PFs to smaller diameters to allow fitting of relative and AMAs for young geological units that do not contain larger craters. To determine whether the PF can be expanded to smaller crater diameters, we studied the CSFDs on ejecta blankets at the four young Copernican-aged craters Giordano Bruno, Moore F, North Ray, and South Ray. The selection of young reference units on ejecta blankets ensures (a) that the CSFDs are in production and have not reached equilibrium at the crater diameters of interest (e.g., Gault, 1970; Melosh, 1989) and (b) possible contrasts in target properties are minimized (e.g., van der Bogert et al., 2017).

In this paper, we perform CSFD measurements on four young Copernican-aged crater ejecta blankets. We analyze the resulting CSFD slopes and evaluate effects such as target properties, crater degradation, secondary craters, and the impactor population. Our results will be compared with literature data.

1.1. The CSFD Slope at Small Crater Diameters

The CSFD slope reflects the number ratio of primary impacts with various magnitudes forming on the lunar surface and can therefore, using crater scaling laws, be used to determine the size-frequency of craters in production and the impactor size-frequency distribution (e.g., Hartmann et al., 1981; Ivanov et al., 2002). The 11th degree polynomial of Neukum (1983) and Neukum et al. (2001) reveals a slope for crater diameters <250 m of −3.82 (cumulative) and for diameters between 10 and 23 m of −3.0 (cumulative). The power laws of Hartmann (1999, 2005) have slopes of −2.2 (log-incremental) for craters >64 km in diameter, −1.80 (log-incremental) for craters between <64 and 1.41 km, and a slope of −3.82 (log-incremental) for craters between <1.41 and 0.3 km.

However, the size distributions of small impact craters are significantly influenced by diverse factors, such as target properties, secondary cratering, crater degradation, and resurfacing processes (e.g., Basilevsky et al., 2018; Fassett et al., 2018; Hiesinger et al., 2012; McEwen & Bierhaus, 2006; Melosh, 1989; Schultz & Spencer, 1979; van der Bogert et al., 2010, 2017, 2018; Wünnemann et al., 2011; Xiao & Strom, 2012; Zanetti et al., 2017). These factors must be evaluated and reduced in order to obtain the most undisturbed CSFD measurement possible. In general, target properties (e.g., strength, porosity, and density of the target material) play an important role for small craters predominantly formed in the strength regime (e.g., Housen & Holsapple, 2011; Melosh, 1989). On the Moon the strength- to gravity transition is somewhat below 1 km (Melosh, 1989; Neukum & Ivanov, 1994; Schultz & Spencer, 1979; van der Bogert et al., 2017). Thus, all craters in this study were formed in the strength regime. That means that, for the same impactor size, crater diameters increase in targets with lower density and less strength, which causes the resulting CSFD to be shifted to slightly larger diameters, but at the same crater frequency (e.g., Housen & Holsapple, 2011; van der Bogert et al., 2017; Wünnemann et al., 2011). This results in older apparent ages and, if the larger diameters do not increase in size at the same rate, a steeper CSFD slope (e.g., van der Bogert et al., 2017). Empirical observations by van der Bogert et al. (2010) indicate that the crater diameter is ∼20% larger in the ejecta material than in the melt pool material of the Jackson crater. Hence, to exclude target property effects in this study, we only determine CSFDs on continuous ejecta deposits.

Secondary craters also affect the CSFD slope (e.g., McEwen & Bierhaus, 2006; Xiao & Strom, 2012; Zanetti et al., 2017). Field-secondaries can be identified by clustering, chains, and herringbone patters (e.g., McEwen & Bierhaus, 2006; Oberbeck & Morrison, 1973; Shoemaker, 1962). However, self-secondary craters can be difficult to detect since they occur irregularly distributed across the surface (e.g., ejecta blankets) and have morphologies

similar to primary craters, which poses the risk of including them in the CSFD measurement (e.g., Plescia et al., 2010; Zanetti et al., 2017). In such cases, the slope becomes steeper than the slope of the primary crater PF (e.g., McEwen & Bierhaus, 2006; Plescia & Robinson, 2011; Zanetti et al., 2017).

The stage of crater degradation is another method to infer the ages of lunar surfaces. It allows a relative chronological classification of the craters, and is used to classify craters into specific degradation stages and linking them to the lunar impactor flux (e.g., Basilevsky, 1976; Basilevsky et al., 2014; Fassett & Thomson, 2014; Soderblom & Lebofsky, 1972; Stöffler et al., 2006). However, besides the time-dependent degradation, processes like mass wasting, seismic shaking, and coverage through impacts (resurfacing) increase the crater degradation stage (e.g., Basilevsky et al., 2014; Drozd et al., 1974; Fassett & Thomson, 2014; Mahanti et al., 2018; Senthil Kumar et al., 2013; van der Bogert et al., 2018; Xiao et al., 2013; Xie et al., 2017). Furthermore, smaller craters degrade faster than large craters, resulting in an uneven degradation stage of craters on a geological unit (e.g., Fassett & Thomson, 2014; Mahanti et al., 2018; Trask, 1971).

The influence of crater degradation on the CSFD slope is twofold: either a high degradation stage might hinder the identification of especially small craters, leading to a reduced number of small craters in the CSFD measurement and a shallower CSFD slope. Or, degradation enlarges the initial crater diameter, resulting in a higher number of large craters in the measured CSFD, resulting in a steeper CSFD slope (Xie et al., 2017).

2. Data and Methods

2.1. Crater and Count Area Selection

We focused on the young Copernican-aged craters Giordano Bruno, Moore F, North Ray, and South Ray, which have a crisp crater rim and ejecta blanket (see Figure 1).

Giordano Bruno (36.0°N, 102.9°E) is about 21.5 km in diameter and is located between Mare Humboldtianum and Mare Moscoviense. Morphologically, it appears to be transitional between simple and complex craters (Plescia et al., 2010). Morota et al. (2009) determined ages of 1–10 Ma for several counting areas on the ejecta and suggested an age of 4 Ma for the impact. Basilevsky and Head (2012) estimated an age between 5 and 10 Ma based on the morphological sharpness of craters superposing Giordano Bruno's ejecta blanket. Its ejecta is relatively smooth and continuous, although in the south it is overprinted by melt deposits.

Moore F (37.3°N, 175.0°W) has a diameter of 23.5 km and is located 60 km east of Moore crater. The ∼41 Ma old crater (Morota et al., 2009) has a central peak, which is surrounded by melt deposits. The ejecta appears smooth with boulders close to the crater rim.

North Ray (8.8°S, 15.5°E) is about 950 m in diameter and is located 5 km north of the Apollo 16 landing site in the Descartes Highlands. The crater has a distinct ejecta blanket and bright rays and plays an important role in constraining the chronology function since rock samples from its vicinity were collected that give exposure ages about 50 Ma (Arvidson et al., 1975; Behrmann et al., 1973; Drozd et al., 1974; Marti et al., 1973; Stöffler & Ryder, 2001).

South Ray (9.1°S, 15.4°E) has a diameter of approximately 700 m and is located 6 km south-west of the Apollo 16 landing site in the Descartes Highlands. With an age of 2 Ma (Arvidson et al., 1975; Behrmann et al., 1973; Drozd et al., 1974; Stöffler & Ryder, 2001), it is a very young simple crater. It has a high-albedo ejecta with an extensive ray pattern.

These four craters were selected to minimize the number of field-secondary craters on the ejecta blanket and to avoid major degradation (e.g., Fassett & Thomson, 2014; H. J. Moore et al., 1980) of small craters. In addition, we focused on young craters so that small craters formed on their ejecta had not yet reached equilibrium. We use the term equilibrium similar to Gault (1970) and Melosh (1989), which defines it as a state of the (lunar) surface where the number of craters is already so high that each newly formed crater destroys, on average, an older crater. For the estimation of the equilibrium of the investigated craters, the standard lunar equilibrium function of Trask (1966) was used. Some of the selected count areas are relatively small due to the strict requirements that count areas must fulfill: The investigated areas need to be representative of the crater of interest and therefore are visually free of resurfacing events and secondary crater clusters, chains, and rays; identified secondary craters were excluded. In addition, we did not include regions in our count areas with topographically steep slopes near

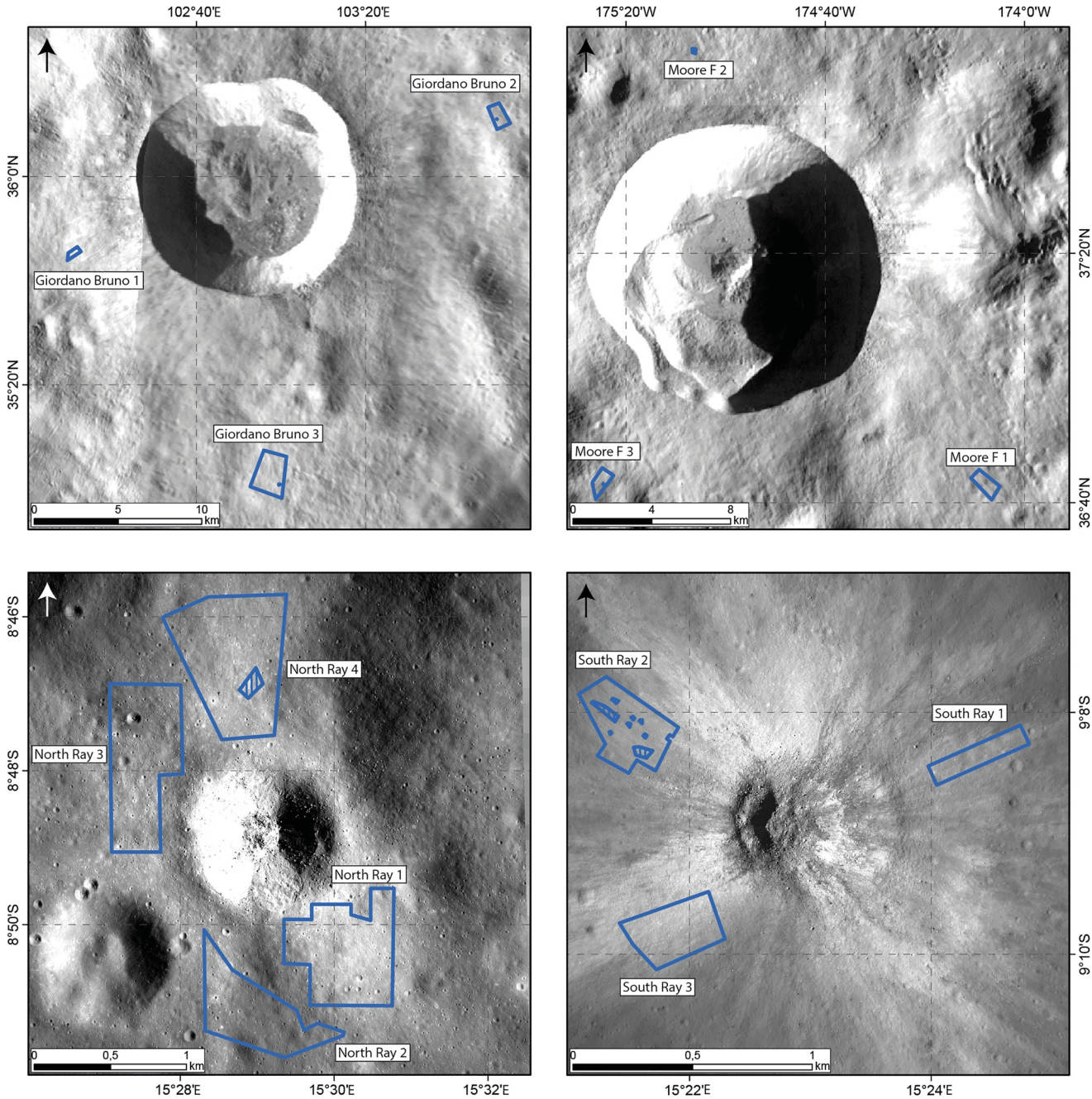

Figure 1. Locations of the study areas where the crater size-frequency distribution measurements were conducted. For the count areas at Giordano Bruno and Moore F (top panels), the Lunar Reconnaissance Orbiter (LRO) Wide Angle Camera mosaic (Robinson et al., 2010) is displayed, and North Ray and South Ray craters (bottom panels) are shown on LRO Narrow Angle Camera mosaics (Table 1, Robinson, 2011). Inlying areas (hatched) are excluded from the count areas.

the crater rim, extensive boulder fields, and areas with rough or rope-like structures. To avoid self-secondary craters as much as possible, some count areas are located at some distance from the crater rims. All count areas were placed in regions of continuous ejecta blanket, where its thickness is large enough to completely cover craters of the underlying substrate in an attempt to minimize the effect when incorporating them into our CSFD (see Section 4.1).

In addition to their formation age, all studied craters are within the highlands to avoid possible effects of compositional and physical differences between different terrain types as these effects may change the size of craters formed on the ejecta blankets.

Table 1
Key Parameters of Lunar Reconnaissance Orbiter Narrow Angle Camera Products Used in Our Study

Count area	Product ID	Observation year	Incidence angle (°)	Phase angle (°)	Pixel scale (m/px)
Giordano Bruno 1	M180509194LE	2012	78.09	79.86	1.59
Giordano Bruno 2	M1122929850LE	2013	65.12	66.84	1.51
Giordano Bruno 3	M103831840LE/RE	2009	64.9/65.13	74.53/71.89	1.54/1.53
Moore F 1	M1107052575RE	2012	62.04	60.99	1.57
Moore F 2	M1112971104RE	2013	64.64	63.49	1.49
Moore F 3	M1112978178LE	2013	65.04	55.19	1.51
North Ray 1	M129187331LE	2010	54.19	55.86	0.49
North Ray 2	M129187331LE	2010	54.19	55.86	0.49
North Ray 3	M129187331LE/RE	2010	54.19/54.26	55.86/53.12	0.49/0.49
North Ray 4	M129187331RE	2010	54.26	53.12	0.49
South Ray 1–3	M119754107RE	2010	56.15	34.79	0.52

We decided to limit the considered crater diameters. Roll-overs occur naturally at small crater diameters during the crater counting process, indicative of the resolution limit of the image used. Therefore, we set the minimum diameter for the small crater diameters in each count area to a bin at which the differential plot does not yet show a roll-over. Crater diameters below that limit are not included in the CSFD slope analysis. Crater diameters, which appear to have reached equilibrium, were excluded as well. Largest crater diameters at North Ray 3, combined North Ray, and Moore F 3 indicate a resurfacing event and are therefore not included in this analysis. The considered crater diameters for each count area are shown in Table 3. For the determination of unidentified secondary craters in our CSFD measurement we use the randomness analysis of Michael et al. (2012), which displays the degree of second neighbor clustering for individual crater bin sizes (Figure 2).

We also ensured that the individual count areas did not cross the Lunar Reconnaissance Orbiter (LRO) Narrow Angle Camera (NAC) image edges with different illumination conditions to eliminate image boundary effects. An exception, however, is for areas Giordano Bruno 3 and North Ray 4 where counts were conducted across the LE/RE boundary of the images (see Table 1). Here, very minorly different pixel scales and incidence angles are present, which should not have a significant influence on the CSFDs. The count areas of North Ray were originally determined by König (1977) and recounted by Hiesinger et al. (2012). We also base our count areas on these previously derived areas, but slight modifications were made to reduce the influence of boulder fields and to avoid possible layering effects.

2.2. Data and Slope Calculation

For our investigation, we used images from the Lunar Reconnaissance Orbiter Narrow Angle Camera (LROC NAC, Robinson, 2011) with pixel scales between 0.5 and 1.6 m/px and incidence angles between 54° and 78° (see Table 1). The images were obtained from the Planetary Data Systems (Robinson, 2011) and processed with the Integrated Software for Imagers and Spectrometers (ISIS, Anderson et al., 2004).

Craters were identified using ArcGIS in combination with the two-point counting tool of CraterTools (Kneissl et al., 2011). The CSFDs were visualized in CraterStats using pseudo-log binning (Michael et al., 2016). Details on how to perform and display CSFD measurements are provided in several studies (e.g., Crater Analysis Techniques Working Group, 1979; Hartmann & Neukum, 2001; Hiesinger et al., 2000; Neukum, 1983; Neukum & Ivanov, 1994; Neukum et al., 2001; Werner & Ivanov, 2015).

We also used slope maps derived from NAC digital terrain models (DTMs, Table 2, Henriksen et al., 2017) to identify flat surfaces to avoid effects of enhanced crater degradation due to slopes on our CSFD measurements. Since only parts of Giordano Bruno are covered with available NAC slope maps and no count areas were covered at Moore F, the Multi-temporal Database of Planetary Image Data (MUTED, Heyer et al., 2018) was used to identify suitable stereo NAC image pairs, from which high-resolution DTMs were calculated using the Ames Stereo Pipeline (Beyer et al., 2018). Finally, the Clementine ultraviolet-visible color ratio composite map of

Table 2
Lunar Reconnaissance Orbiter Narrow Angle Camera Images Used to Generate Digital Terrain Models (DTMs) and Existing DTM Products Utilized in Our Study, From Which Slope Maps Were Made

Count area	NAC product ID/*DTM product ID	NAC pixel scale (m/px)	DTM pixel scale (m/px)
Giordano Bruno 1	M1100516110LE/RE	1.22/1.20	3.66
	M1100537548LE/RE	1.17/1.17	
Giordano Bruno 2	M1207693791LE/RE	1.20/1.19	3.60
	M1207714892LE/RE	1.16/1.17	
Giordano Bruno 3	NAC_DTM_GIORDNBRNO*		3.00
Moore F 1	M1120031479LE/RE	1.24/1.23	3.81
	M1120038581LE/RE	1.27/1.26	
Moore F 2	M1112956872LE/RE	1.58/1.56	4.74
	M1112978178LE/RE	1.51/1.52	
Moore F 3	M1112956872LE/RE	1.58/1.56	4.74
	M1112978178LE/RE	1.51/1.52	
North Ray 1-4	NAC_DTM_APOLLO16*		2.00
South Ray 1-3	NAC_DTM_APOLLO16*		2.00

Note. The given DTM pixel scales were used to derive slope maps.

Lucey et al. (2000) was used to ensure that the count areas for a given crater have similar and homogeneous compositional properties.

The CSFD slopes were calculated with the algorithm of Clauset et al. (2009). This algorithm uses a combination of the goodness-of-fit test and maximum likelihood estimators and fits a power law onto the unbinned data. As it only requires the diameter of each crater and is independent of the display of the data, it is statistically more robust and less biased than fitting a power law onto binned data (Clauset et al., 2009; Robbins et al., 2018). However, the algorithm of Clauset et al. (2009) is intended to fit the entire diameter range of the measured data rather than only considering specific diameter ranges. We found no differences in CSFD slope when crater diameters indicating a resurfacing are included (e.g., North Ray 3), except that the uncertainty is larger.

3. Results

We investigated several areas on Giordano Bruno, Moore F, North Ray, and South Ray in order to analyze the slope of small crater distributions, particularly craters ≤10 m. The CSFDs are shown as cumulative and R-plots (see Figure 2, Crater Analysis Techniques Working Group, 1979).

3.1. Analyses of CSFD Measurements

The CSFD measurements indicate a slope of about −3 for craters ≤10 m and slightly steeper slopes for craters between 10 and 20 m compared with Neukums −3 slope in the same crater diameter range (Neukum, 1983; Neukum et al., 2001).

The cumulative plots for Giordano Bruno 1 and Giordano Bruno 2 show a small kink at 10 m crater diameter. For these count areas, the slope of the larger craters is shallower than the slope of the smaller craters (see Figure 2 and Table 4). Giordano Bruno 3 shows no kink and has as well a generally steep slope, but with a steeper slope for the larger crater diameters than for the smaller crater diameters. The slope changes are also well seen in the R-plots. In the studied count areas, craters reach equilibrium at diameters between 6 and 8 m. Randomness analyses indicate that unidentified secondaries are present at crater diameters ≤8 m.

The CSFDs of the Moore F 1 and Moore F 2 count areas do not show any resurfacing kinks. For the count area Moore F 3, the slope of the CSFD changes at 25 m. The individual CSFD measurements, as well as the combined data set for all the measurements, align well with each other in the R-plot. For the Moore F count areas, equilibrium is reached at a crater diameter of <5 m. The randomness analyses show that the investigated crater diameter range (5–67.2 m) does not include obvious crater clusters.

The CSFD measurements at North Ray 1, North Ray 2, and North Ray 4 do not display any resurfacing events and show a smooth CSFD within the considered crater diameters (6–41.7 m, see Table 3). North Ray 3 and the combined measurements indicate a resurfacing and are therefore limited to 30 and 40 m, respectively. The scattering of the individual and combined count areas in the R-plot slightly increases for larger crater diameters, where the number of craters is low. The North Ray CSFDs indicate that equilibrium is reached at a crater diameter <5–6 m. The randomness analysis shows no clustering, hence secondary craters are sparse.

The CSFDs of South Ray show no obvious resurfacing. The R-plot is relatively scattered for the individual and combined CSFD measurements, but nevertheless indicates an alignment which each other in the considered crater diameter range. The measured craters for the South Ray count areas are not in equilibrium, and the randomness analysis shows no crater clustering.

Table 3 shows the individual count areas with relevant parameters, such as the area size, considered crater diameter range, number of craters, the $N(0.01)$ value, and the error of $N(0.01)$. Since the investigated crater diameters are small, we decided to deviate from reporting the usual $N(1)$ or $N(10)$ values, which indicate crater density at ≥1

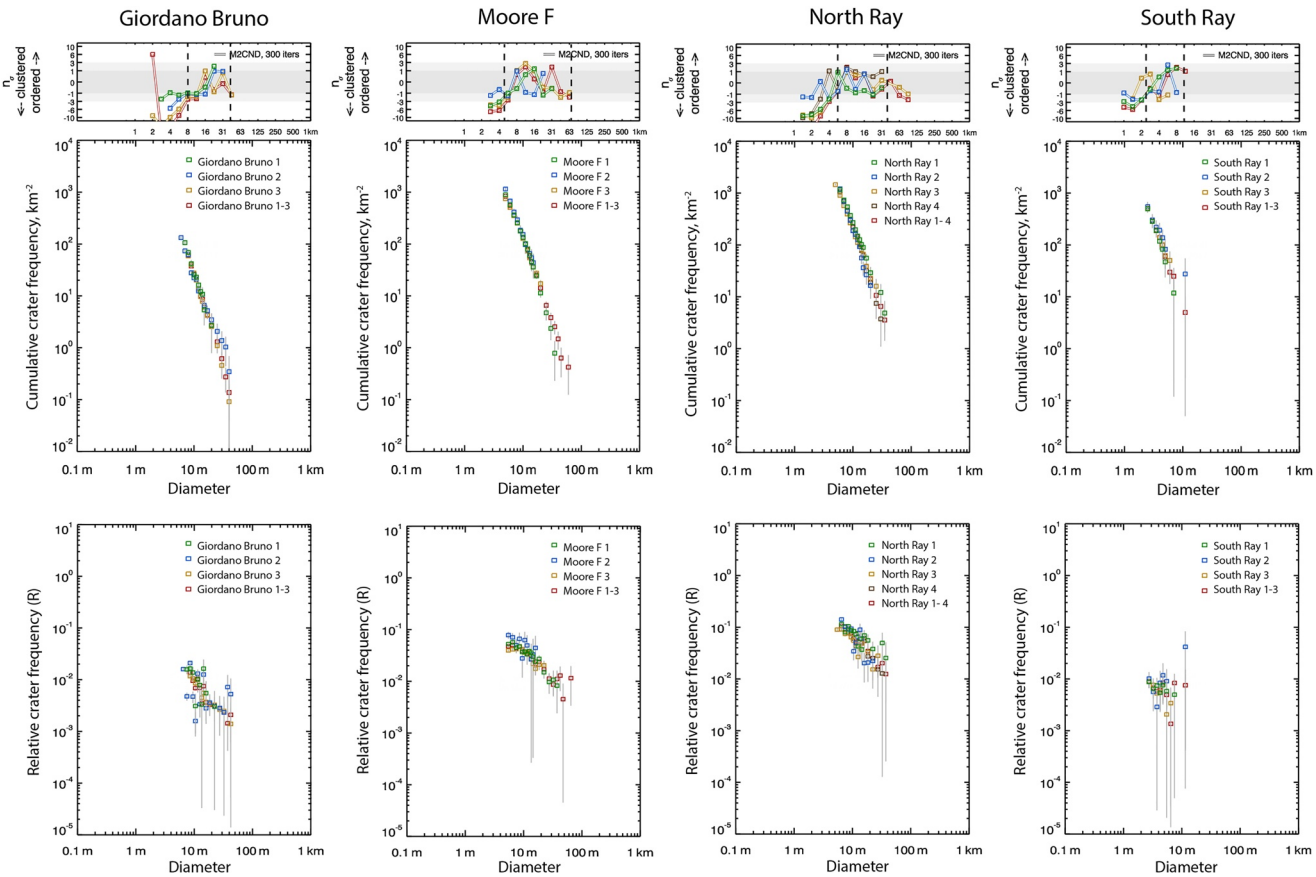

Figure 2. Crater size-frequency distribution measurements of the investigated areas displayed as cumulative (center row) and R-plots (bottom row). The black dashed lines in the randomness analyses (top row) show the crater diameter ranges selected for further analysis (see Table 3). Vertical gray lines on individual data points are the error bars. The randomness analyses show that the selected diameter ranges are not affected by clusters of unidentified secondary craters.

or ≥10 km, respectively. Instead, we report $N(0.01)$ or the frequency of craters at ≥10 m in diameter, thus reducing potential errors when small craters with diameters ≥10 m are extrapolated to a CSFD at ≥1 km. An accuracy assessment for $N(0.01)$ values is provided in Section 4.5. In our study of the CSFD slopes on ejecta blankets of young Copernican-aged craters, we investigated craters with diameters between 2.5 and ~67 m.

3.2. Analyses of CSFD Slopes

The slopes of the individual and combined study areas were assessed in crater diameter ranges and as a whole, with crater diameter ranges ≤10 m, between 10 and 20 m, which allows a direct comparison with the CSFD slope of −3 derived by Neukum (1983) and Neukum et al. (2001), ≥10 m, and across the full considered crater diameter range. We also examined the CSFDs from the combined count areas for each of the individual study craters, as these all represent the same geological units (Hiesinger et al., 2012).

In the following analysis, we compare our CSFD slopes to the nominal −3 slope of Neukum (Neukum, 1983; Neukum et al., 2001) in the crater diameter range of 10–20 m; thus, we refer to "shallower" slopes if our determined CSFD slopes were greater −3 and to "steeper" slopes if they are below −3. The similarity between the CSFD slope of craters ≤10 m and the full crater diameter range, as well as between craters ≥10 and 10–20 m, results from the more abundant smaller craters, which are therefore more heavily weighted.

In general, the count areas at Giordano Bruno show very steep slopes in every diameter range. For Giordano Bruno 1, Giordano Bruno 2, and combined Giordano Brno, the slope at smaller crater diameters is steeper than for larger diameters, particularly for Giordano Bruno 1. Giordano Bruno 1 has a steep slope of −3.92 for craters ≤10 m, and at larger crater diameters, the slope is −3.28. Giordano Bruno 2 also has a slope above −3 at craters ≤10 m and a shallower slope of −2.69 considering larger crater diameters. Giordano Bruno 3 has a steeper slope

Table 3
Parameters Derived From the Crater Size-Frequency Distributions

Count area	Area (km)	Crater diameter range (m)	Number of craters	$N(0.01)$ (km^{-2})	Error $N(0.01)$ (km^{-2})
Giordano Bruno 1	0.744	7–25.8	78	3.23×10^{1}	3.66
Giordano Bruno 2	2.90	6–43.4	385	2.72×10^{1}	1.39
Giordano Bruno 3	11	8–44.9	647	2.71×10^{1}	1.07
Combined Giordano Bruno	**14.6**	**8–44.9**	**879**	$\mathbf{2.69 \times 10^{1}}$	$\mathbf{9.07 \times 10^{-1}}$
Moore F 1	2.55	5–38.2	2273	1.14×10^{2}	2.39
Moore F 2	0.092	5–27.2	104	1.46×10^{2}	1.43×10^{1}
Moore F 3	2.09	5–25	1,543	1.14×10^{2}	2.90
Combined Moore F	**4.73**	**5–67.2**	**3,939**	$\mathbf{1.19 \times 10^{2}}$	**1.90**
North Ray 1	0.411	6–41.7	475	2.64×10^{2}	1.21×10^{1}
North Ray 2	0.301	6–26.5	363	2.34×10^{2}	1.23×10^{1}
North Ray 3	0.437	5–30	633	1.96×10^{2}	7.79
North Ray 4	0.533	6–35.2	560	2.33×10^{2}	9.85
Combined North Ray	**1.68**	**6–40**	**1,795**	$\mathbf{2.31 \times 10^{2}}$	**5.45**
South Ray 1	0.0845	2.5–8	42	7.75	1.20
South Ray 2	0.0363	2.5–11.8	20	9.86	2.20
South Ray 3	0.0796	2.5–7.4	38	8.43	1.37
Combined South Ray	**0.2**	**2.5–11.8**	**103**	**8.28**	$\mathbf{8.16 \times 10^{-1}}$

Note. The $N(0.01)$ values are based on the PF of Neukum (1983). The bold values represent the combined data.

at craters ≥10 m and a shallower slope with −3.50 at craters ≤10 m. The combined CSFD at Giordano Bruno has a steep slope (−3.55) at craters ≤10 m and across the full diameter range, the slope at ≥10 m and between 10 and 20 m is with −3.43 slightly shallower.

The CSFDs at Moore F exhibit a different trend, with a shallower slope at smaller crater diameters and a steeper CSFD slope at larger crater diameters. Moore F 1 has a slope of −2.74 at craters ≤10 m and a slope of −3.33 considering the larger crater diameters. Moore F 2 has a slope of −3.01 for the smaller crater diameters and across the full crater diameter range, but a steeper slope of −3.63 for crater ≥10 m and between 10–20 m. Moore F 3 as generally a shallow slope for craters ≤10 m and across the full crater diameter range (−2.45), and a slope of −2.97 for craters ≥10 m and between 10 and 20 m. The combined areas show a relatively shallow slope (−2.62) at craters ≤10 m, and a slope of −3.16 at craters ≥10 m and between 10 and 20 m.

North Ray 1 shows slopes varying around −3, whereas the crater diameters ≤10 m and across the full diameter range are slightly below −3 (−2.88). In the diameter range ≥10 m and between 10 and 20 m, we observe a slope of −3.14. The slopes at North Ray 2 are generally steep, with −3.55 for craters ≤10 m and across the full crater diameter range, and −3.39 for craters ≥10 and 10–20 m. North Ray 3 has shallower slopes between −2.78 (≤10 m and across the full crater diameter range) and −2.67 (≥10 and 10–20 m). North Ray 4 has a slope of ∼−3 at craters ≤10 m and a steepe slope at craters ≥10 m (−3.34). The combined count areas at North Ray exhibit a similar trend to Moore F with shallower slopes at smaller crater diameters (−3.03 at craters ≤10 m, and −3.10 at craters between 10 and 20 m).

South Ray 1 and South Ray 3 do not have craters ≥10 m. They have steep CSFD slopes of −3.84 and −3.14, respectively for craters ≤10 m. South Ray 2 has a CSFD slope of −2.63 for craters ≤10 m and across the full crater diameter range, and a steep slope of −3.90 for craters ≥10 m and between 10 and 20 m. The combined count areas at South Ray have a slope of −3.08 at crater diameters ≤10 m and the full diameter range, and −3.20 for craters ≥10 m and between 10 and 20 m.

4. Discussion

We observed the following trends in the CSFDs of Moore F, North Ray, and South Ray craters: crater diameters ≤10 m fit a −3 slope very well, whereas larger crater diameters (10–20 m, ≥10 m) are slightly steeper than −3.

Table 4
Slope Comparison in Diameter Ranges ≤10, 10–20, ≥10 m, and Across the Entire Diameter Range

	Slope			
Count area	≤10 m	≥10 m	10–20 m	Full diameter range
Giordano Bruno 1	−3.92	−3.28	−3.28	−3.92
Giordano Bruno 2	−3.32	−2.69	−2.69	−3.32
Giordano Bruno 3	−3.50	−3.68	−3.68	−3.50
Combined Giordano Bruno	**−3.55**	**−3.43**	**−3.43**	**−3.55**
Moore F 1	−2.74	−3.33	−3.33	−2.74
Moore F 2	−3.01	−3.63	−3.63	−3.01
Moore F 3	−2.45	−2.97	−2.97	−2.45
Combined Moore F	**−2.62**	**−3.16**	**−3.16**	**−2.62**
North Ray 1	−2.88	−3.14	−3.14	−2.88
North Ray 2	−3.55	−3.39	−3.39	−3.55
North Ray 3	−2.78	−2.67	−2.67	−2.78
North Ray 4	−2.97	−3.34	−3.34	−2.97
Combined North Ray	**−3.03**	**−3.10**	**−3.10**	**−3.03**
South Ray 1	−3.84			−3.84
South Ray 2	−2.63	−3.90	−3.90	−2.63
South Ray 3	−3.14			−3.14
Combined South Ray	**−3.08**	**−3.10**	**−3.10**	**−3.08**

Note. The smallest and largest considered crater diameters are given in Table 3. The bold values represent the combined data.

In contrast, Giordano Bruno shows a steeper CSFD slope at craters ≤10 m (−3.55) and a slightly shallower slope, but still above −3, at larger crater diameters.

Considering only diameters from 10 to 20 m, we calculated an average CSFD slope of −3.20 across all combined count areas at Giordano Bruno, Moore F, North Ray, and South Ray. This is slightly steeper than Neukum's −3 slope (Neukum, 1983; Neukum et al., 2001) in the same crater diameter range. For craters ≤10 m we derived an average CSFD slope of −3.07 when taking Giordano Bruno into account, although its CSFD slopes are significantly steeper than −3. For Giordano Bruno, several authors (including ourselves) found a steep CSFD slope, which has been interpreted to be the result of secondary cratering (e.g., Plescia & Robinson, 2019; Plescia et al., 2010; Williams et al., 2022) or crater degradation (Xie et al., 2017). As described, for example, in Zanetti et al. (2017), there is a high variability of crater densities across ejecta blankets, which may result from self-secondary cratering. These self-secondaries cannot be easily separated from primary craters based on their morphological characteristics. However, our count areas were selected carefully and secondary clusters and rays were excluded. Despite this, random secondaries, which could not be identified based on their morphology, may have been unintentionally included in our CSFD measurements. However, secondary contributions to the CSFD plot can be further minimized in the randomness analyses by excluding bins that show clustering (see Figure 2). Thus, if we interpret Giordano Bruno's extraordinarily steep CSFD slopes with caution in the diameter range of ≤10 m and exclud these CSFD measurements in the final result, we derive an average slope of −2.91.

Generally, our count areas might be affected by target properties and crater degradation, which is discussed in Section 4.1 and Section 4.2, respectively. Steep CSFD slopes might be associated with secondary cratering and are covered in Section 4.3. Another possibility might be that the determined CSFDs reflect the impactor population (see Section 4.4). For the comparison with other authors, we translate their provided $N(1)$ values to our used $N(0.01)$ (see Table 5).

Comparing our $N(0.01)$ values using the PFs of Neukum (1983) and Neukum et al. (2001) with the literature data, we generally find a good agreement. Morota et al. (2009) found an $N(0.01)$ of 14.7, which represents

Table 5
Comparison of Crater Frequencies N(0.01) for the Studied Craters Using the Production Function of Neukum (1983) (*) and Neukum et al. (2001) (**)

	Giordano Bruno $N(0.01)$	Moore F $N(0.01)$	North Ray $N(0.01)$	South Ray $N(0.01)$
This work*/**	24.5/24.5	130/129	222/222	6.65/6.70
König (1977)** (taken from Robbins (2014))			176	
H. J. Moore et al. (1980)** (taken from Robbins (2014))			272	
Neukum (1983) and Neukum and Ivanov (1994)*			202	
Morota et al. (2009)*	14.7	160		
Hiesinger et al. (2012)**			175/170	
Xiao and Strom (2012)**	6.80			
Robbins (2014)**			272	5.57
Plescia and Robinson (2019)**	19–183			
Williams et al. (2022)**	23.92			

Note. $N(1)$ values from the literature have been converted to $N(0.01)$ values. All N-values were measured at binned craters. Note that we only have one crater to determine the $N(0.01)$ value of South Ray.

fewer craters than our results, which show $N(0.01) = 24.5$ at Giordano Bruno. Xiao and Strom (2012) found an even lower crater frequency of 6.80. Our results fit well with the $N(0.01)$ value of 23.92 derived by Williams et al. (2022). Plescia and Robinson (2019) investigated several areas and derived $N(0.01)$ values between 19 and 183. For Moore F, our newly derived $N(0.01)$ value of 130 agrees well with Morota et al. (2009), who derived an $N(0.01)$ value of 160 using the PF of Neukum (1983). For North Ray, our value ($N(0.01) = 222$) is lower than the crater frequencies reported by Moore et al. (1980) and Robbins (2014), who derived an $N(0.01)$ of 272, and higher than Neukum (1983) and Neukum and Ivanov (1994) who reported an $N(0.01)$ value of 202. The values of König (1977) ($N(0.01) = 176$) and Hiesinger et al. (2012) ($N(0.01) = 175/170$) reflect lower crater frequencies. We have only one crater ≥10 m at South Ray, which gives us an $N(0.01)$ of 6.65/6.70, which is relatively similar to Robbins (2014) with their $N(0.01) = 5.57$. Note that one crater provides a very low statistic and has only a limited meaning.

A direct comparison of our CSFD slopes with slopes from the literature (Table 5) is complicated by differently chosen diameter ranges in the respective publications. H. J. Moore et al. (1980) found the slope at North Ray and Cone Crater to be −2.8 for craters between 4 and 50 m and compared the slope with Shoemaker (1965). Xie et al. (2017) found an overall slope of −3.2 for craters <∼1 km, when taking influences from the enlargement of crater diameters due to crater degradation into account (see Section 4.2).

Ivanov (2006), using the chronology system of Neukum et al. (2001), states that age determination for crater diameters <10 m older than 30 Ma is impossible since these craters have already reached equilibrium. Craters with diameters of 10 m and age of 30 Ma have a $N(0.01)$ of 110 in the chronology system of Neukum et al. (2001). North Ray exceeds this value ($N(0.01) = 222$, Table 5). However, our investigation shows that CSFD measurements at North Ray have not yet reached equilibrium and thus provide valuable information for a potential extension of a PF.

4.1. Target Properties

Since we investigated craters ≤67.2 m, which form in the strength regime (Melosh, 1989; Neukum & Ivanov, 1994; Schultz & Spencer, 1979; van der Bogert et al., 2017), target properties play an important role in the final crater diameters and should be considered. The investigated CSFDs were measured exclusively on the ejecta blankets of Giordano Bruno, Moore F, North Ray, and South Ray. This approach was chosen to reduce the effects of contrasting target properties on the studied craters by restricting the CSFD measurements to a single terrain type. However, impactors penetrating through the ejecta deposits do create different crater diameters in the strength regime due to layering and the contrast in target properties between the layers (Wünnemann et al., 2012), which could cause a variation in the CSFD slopes. Hence, we investigated whether the craters measured for the CSFDs are large enough to penetrate the ejecta deposits (Figure 3). According to Gault (1970) and Wünnemann et al. (2011), the depth-to-diameter ratio of simple craters is about 1/5. We used this relationship to estimate the impact depth of craters forming on the ejecta blankets of our target craters. The ejecta thickness is calculated with the equation of Krüger et al. (2017):

$$E_T = 5.73\,(\pm 0.80) * R_F^{0.399} * \left(\frac{r}{R_F}\right)^{-3.0}$$

with E_T as the ejecta thickness (in m), R_F as the final crater radius (in m), and r as the distance from the crater center (in m).

The plot in Figure 3 visualizes the normalized ejecta thickness and the height of crater floors relative to the ejecta surface at their location for the craters formed on the ejecta blankets. Each vertical line between the ejecta curve and the 0-line reflects a crater that formed completely in the ejecta blanket material. This is the case for all the craters at Giordano Bruno, Moore F, and South Ray. Some purple vertical lines representing individual craters on the North Ray ejecta blanket are below the 0-line and thus penetrate the ejecta blanket. Breaking down this result by count areas, it is evident that no craters have certainly penetrated and that two craters (0.04%) might have penetrated the ejecta blanket, based on the error in the ejecta thickness equation of Krüger et al. (2017), at count area North Ray 1. Count area North Ray 2 has one crater penetrating the ejecta blanket (0.02%) and five craters (0.1%) potentially penetrating the ejecta blanket. North Ray 3 has four craters (0.09%), which might penetrate through the ejecta blanket. Since ∼0.1% of the craters on the individual count areas are or might be influenced,

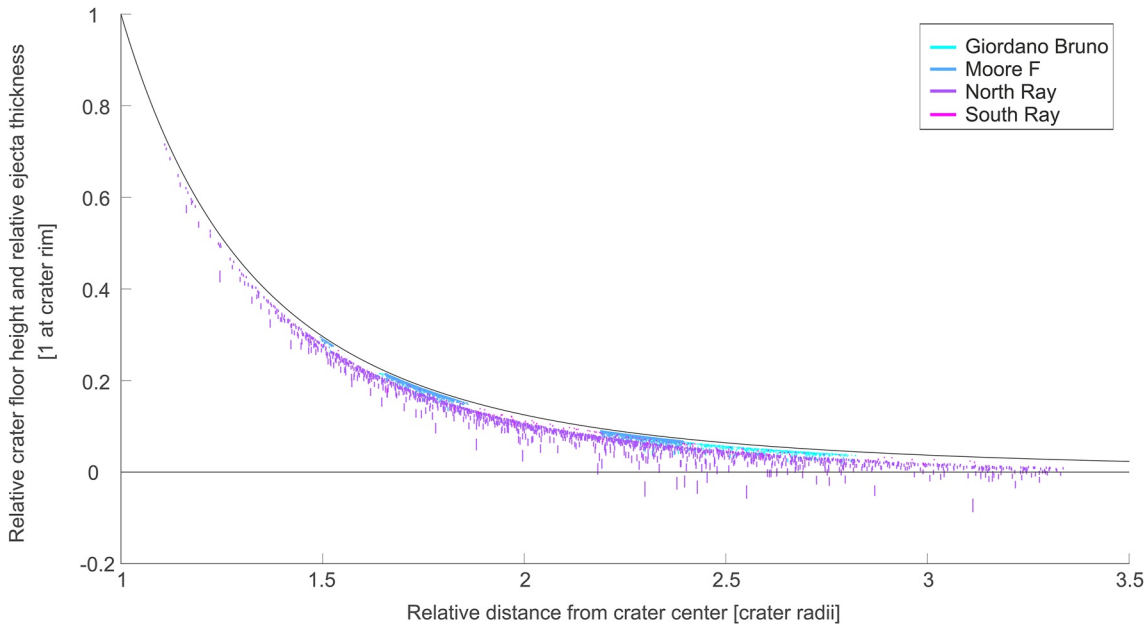

Figure 3. Normalized ejecta thickness with distance from the crater center, showing penetration depths for individual craters in our count areas (turquoise = Giordano Bruno, blue = Moore F, purple = North Ray, and pink = South Ray). The ejecta surface is the black curve. Vertical lines below the 0-line indicate a penetration through the ejecta blanket. The vertical lines represent the error bars of the individual crater floor depths in the count areas, after Krüger et al. (2017).

we expect that the possible effects of layering on the final crater size and the CSFD slope are negligible. Count area North Ray 4 contains 19 craters (0.2%) that are modeled to penetrate through the ejecta blanket and 28 craters (0.3%) that might do so. Here as well, we conclude that an effect on the CSFD measurement is minor.

4.1.1. Ejecta Coverage From Nearby Craters

Another consideration is whether ejecta from nearby impacts could cover smaller craters in our study area and influence the visibility of the smallest craters. North Ray, for example, could be affected by ejecta material from the 8.3 km distant South Ray crater. Drozd et al. (1974) discussed that impact material of Baby Ray could influence areas of South Ray 2.3 km away. However, no resurfacing is visible in the CSFDs and the spectral Clementine data. For Giordano Bruno and Moore F, we found no craters that could have affected their ejecta blanket.

4.1.2. Regolith Thickness

Regolith can play an important role when considering craters with small diameters. Either successive coverage of craters by regolith can obliterate some of the craters and, hence, lead to an undercount, which yields shallower slopes of the CSFDs, or it may result in changes in target properties. Therefore, we considered whether and how the regolith formation might have influenced our CSFD measurements of small craters (Table 6).

In order to investigate newly formed regolith after the impact, we used the equation of Arvidson et al. (1975), who analyzed boulder tracks and proposed a regolith deposition rate of 5 ± 3 cm/Ma in depressions located on slopes, and calculated a regolith thickness at the investigated craters (Table 6). Our results show that the regolith

Table 6
Calculated Regolith Thicknesses Based on Arvidson et al. (1975) for the Investigated Craters

	Calculated regolith thickness on ejecta deposits (m) (Arvidson et al., 1975)		
Crater	min	med	max
Giordano Bruno	0.13	0.32	0.51
Moore F	0.62	1.55	2.48
North Ray	0.93	2.33	3.73
South Ray	0.05	0.12	0.19

at Giordano Bruno and South Ray is relatively thin, when using age determination by radiometric dating (see Section 2.1). Moore F and North Ray have accumulated a thicker regolith. It is, however, not possible to identify individual craters in our CSFD measurements, which are affected by this change in material. In addition, no kink is visible in the CSFD plots (see Figure 2) for the considered crater diameter range (Table 3), which could reflect material differences between the ejecta material and the superposed regolith.

4.2. Crater Degradation

A plausible explanation for shallower slopes at smaller crater diameters might also be that these craters could not be well identified in the images due to their degradation states. Morphological characteristics of degraded craters are a less or non-distinct ejecta blanket, reduced sharpness of the crater rim (Mahanti et al., 2018), reduction of the rim height, downslope movement along the crater walls, and material infill into the crater (Ross, 1968). The last two characteristics cause reduced slopes of the crater walls. From previous investigations, for example, by Trask (1971), Fassett and Thomson (2014), and Mahanti et al. (2018), it is known that small craters degrade faster than larger craters. This effect was investigated in detail by Mahanti et al. (2018), who studied small lunar craters between 35 and 250 m in diameter. They found that crater degradation can complicate the identification and accurate measurements of craters because it enlarges the observed crater diameter (Xie et al., 2017) and makes craters shallower (Basilevsky et al., 2014) so that they blend into the surrounding environment. As a consequence, fewer smaller craters are counted, resulting in a shallower CSFD slope.

Crater degradation correlates, among other external influences, with crater diameter, target material, topography, and time (e.g., Dundas & McEwen, 2007; Fassett et al., 2018; Minton et al., 2019; Richardson et al., 2005; Xie et al., 2019). Fassett and Thomson (2014) derived a global erosion rate of 0.4 mm/Ma in the last 3 Ga in lunar maria. Dundas and McEwen (2007) stated a crater erasure rate, which they define as the destruction of craters by crater infill or mass wasting, of 2–6.6 cm/Ma on the lunar highlands. Craters formed completely within the regolith have a reduced strength of the crater walls compared to basaltic maria, which results in a faster degradation in weak targets (van der Bogert et al., 2017). Xie et al. (2017) investigated the topography degradation of crates and found that smaller craters grow larger faster than larger craters (Mahanti et al., 2018; Xie et al., 2017). Considering the entire lifetime of craters, Minton et al. (2019) stated that smaller craters experience a lower degradation rate in total.

In general, the effects of crater degradation on our CSFD slopes could be twofold: (a) a high degradation stage might hinder the identification particularly of small craters, leading to a reduced number of small craters in the CSFD measurement, and hence, a shallower CSFD slope and (b) the degradation enlarges the initial crater diameter more at smaller diameters than at larger diameters, resulting in a higher number of larger craters in the measured CSFD, which result in a steeper CSFD slope (Xie et al., 2017). We selected areas on young Copernican-aged crater ejecta blankets where indications for significant degradation is low to reduce uncertainties due to time-dependent crater degradation.

4.2.1. Mass Wasting

Mass wasting is especially prominent in areas with steep slopes where downslope movement is frequent (e.g., avalanches and landslides, Basilevsky et al., 2014; Senthil Kumar et al., 2013; Xiao et al., 2013). Basilevsky et al. (2014) proposed that rapid crater degradation through mass wasting is present at crater walls steeper than ~25°. We used LROC NAC DTM slope maps to investigate the slopes of crater walls of impacts formed on the ejecta blankets of Giordano Bruno, Moore F, North Ray, and South Ray (Figure 4). Mass wasting from the crater rims would result in an enlargement of the crater diameter (Xie et al., 2017) and affect the measured crater diameter and the resulting CSFDs.

At Giordano Bruno and Moore F, we do not see individual craters with steep crater rims formed on the ejecta blanket of the respective crater. At North Ray, very few large craters on the ejecta blanket have rims of ≥25°, which would favor crater degradation due to mass wasting processes. South Ray does not show craters with steep rims on its ejecta blanket. Note, that the resolution of the slope maps (see Table 2) is not high enough to identify the slope of the small crater distribution.

Avalanches and landslides can also occur outside craters if the slope exceeds the angle of repose. To assess whether mass wasting processes were likely in our count areas, we reviewed the slopes in these areas. However,

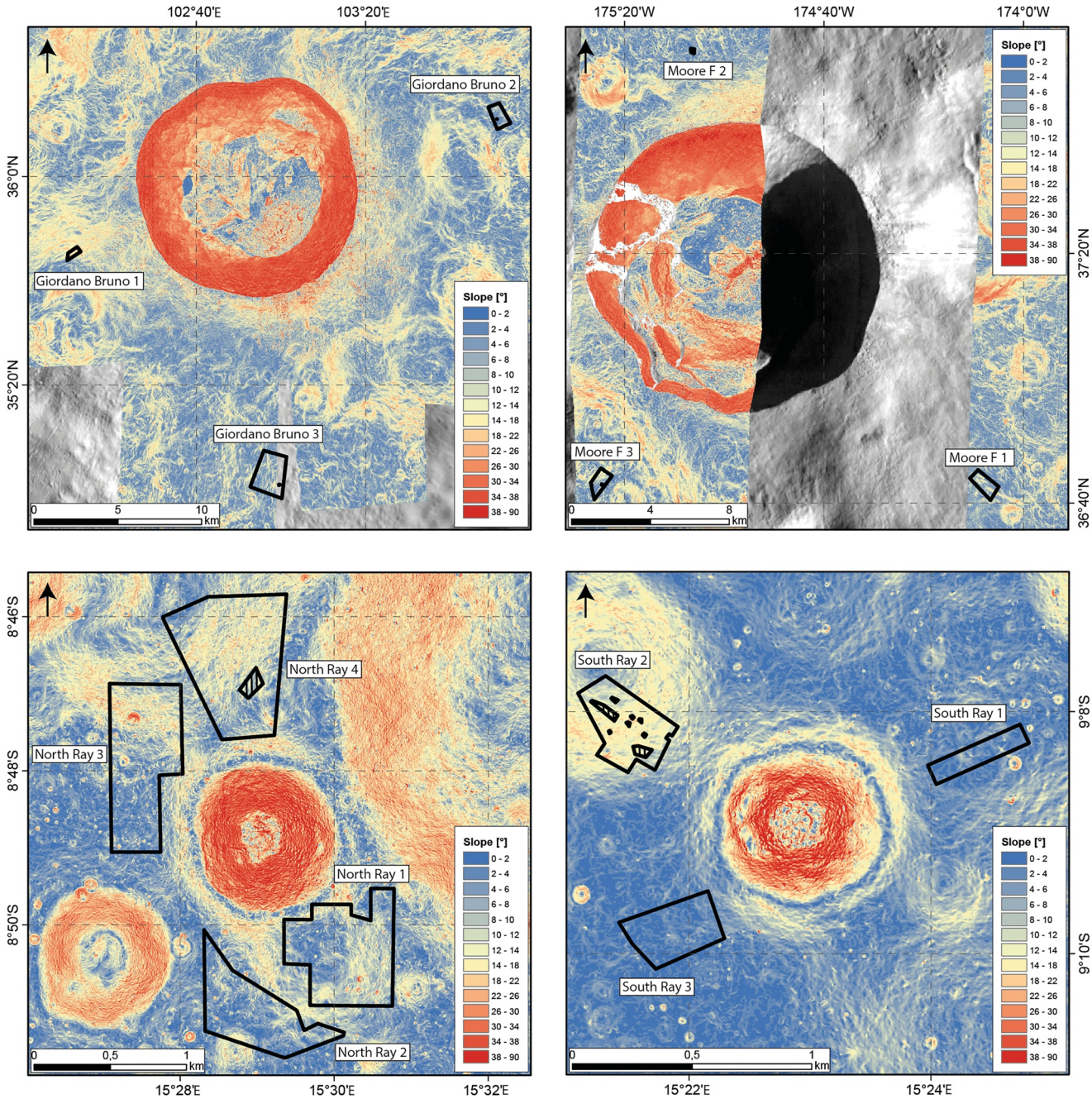

Figure 4. Slope maps of the count areas. The map pixel scale is provided in Table 2. Hatched areas were excluded from the count areas.

our slope calculation is close to the resolution limit and can only be seen as an orientation. The slope maps in Figure 4 show only a small number of surfaces, which have terrain slopes ≥25°. The slopes ≥25° was found at North Ray 3, covering ~1.2% of the total count area. The remaining count areas have significantly lower percentages of terrain slopes ≥25° in relation to the total area.

However, no indications for landslides and avalanches could be identified, neither with the slope maps nor in the panchromatic NAC images. Xiao and Strom (2012) investigated crater density differences in Giordano Bruno's ejecta blanket and concluded that mass wasting was probably not responsible for these density differences.

Table 7
Display of Crater Degradation Mechanisms That Might Affect Individual Study Areas

Area	Age (Ma)	Erasure[a] (m)	Mass wasting seen in NAC images	Seismic shaking	
				Impact related	Tectonically related
Giordano Bruno 1	4	0.26	No	No	No
Giordano Bruno 2			No	No	No
Giordano Bruno 3			No	No	No
Moore F 1	41	2.71	No	No	No
Moore F 2			No	No	No
Moore F 3			No	No	No
North Ray 1	50	3.30	No	Possibly yes	No
North Ray 2			No	Possibly yes	No
North Ray 3			No	Possibly yes	No
North Ray 4			No	Possibly yes	No
South Ray 1	2	0.13	No	Possibly yes	No
South Ray 2			No	Possibly yes	No
South Ray 3			No	Possibly yes	No

[a]The crater erasure rate is taken from Dundas and McEwen (2007) with 0.66 m/Ma for craters with a diameter of 37 m on the lunar highlands.

4.2.2. Seismic Shaking

Seismic shaking can be induced by nearby impacts and may contribute to crater degradation (Mahanti et al., 2018; Nakamura et al., 1979; Richardson et al., 2004, 2005; Titley, 1966; van der Bogert et al., 2018). Thus, we consider whether our study craters may have been affected by such processes. As discussed in Section 4.1.1, North Ray and South Ray craters may have been affected by ejecta from South Ray and Baby Ray craters, respectively (Drozd et al., 1974); thus, due to their proximity, they may have also had seismic effects in addition to ejecta emplacement. In addition, we examined whether there are tectonic sources (e.g., Watters et al., 2015, 2019; Weber et al., 2009) of seismic shaking in the vicinity of our study areas because it has been shown that seismic shaking during the scarp formation can affect small crater CSFDs (van der Bogert et al., 2018). Thus, we used the Quickmap (quickmap.lroc.asu.edu) lobate-scarp map (Nelson et al., 2014) to identify whether our study areas are in the vicinity of such thrust faults. We conclude that Giordano Bruno, Moore F, North Ray, and South Ray do not have lobate scarps or wrinkle ridges in their vicinity; hence, seismic effects on our CSFD should be negligible.

4.2.3. Comparison of Crater Degradation Processes

As discussed in this section, factors such as crater diameter, target material, topography, exposure time (e.g., Dundas & McEwen, 2007; Fassett et al., 2018; Minton et al., 2019; Richardson et al., 2005; Xie et al., 2019), mass wasting (e.g., Basilevsky et al., 2014; Xie et al., 2017), and seismic shaking (van der Bogert et al., 2018) can affect the degradation of craters. To estimate, if our count areas are significantly affected by degradational processes, we searched for evidence in each count area. Our assessment is summarized in Table 7.

Comparing the erasure rate (Dundas & McEwen, 2007) and the regolith accumulation rate (Arvidson et al., 1975), we see that they roughly balance each other out. Mass wasting processes are relevant for slopes of ≥25° (Basilevsky et al., 2014). Steep slopes are present in some areas (see Table 7, Figure 4); however, the proportion is small in relation to the total area. In the panchromatic NAC images, no evidence for mass wasting processes was found in any of our count areas. Note that the slopes at the crater walls might be understated, as the pixel resolution of the slope maps is not high enough. Mahanti et al. (2018) suggested that fresh craters with diameters between 35 and 250 m experience faster mass wasting processes, which in turn reduce diffusive crater degradation. Seismic shaking can be induced by impacts (Nakamura et al., 1979; Richardson et al., 2004, 2005; Titley, 1966) or tectonically active features, such as lobate scarps (van der Bogert et al., 2018; Watters et al., 2019) or failure planes (Weber et al., 2009). However, no lobate scarps were found close to the investigated craters.

4.3. Secondary Craters

We carefully selected our count areas to minimize the effects of field secondary craters. In particular, our count areas are located on the ejecta blankets of Copernican-aged craters because they are least affected by the subsequent emplacement of craters and their secondaries. J. M. Moore and McEwen (1996) listed 31 Copernican-aged craters on the lunar farside, which were identified with Clementine data. We did not find evidence that our count areas were covered by ejecta or rays from any of these craters. Singer et al. (2020) studied the size and frequency of secondary craters as a function of the size of the primary crater. They found that the size and frequency of secondary craters decreases more rapidly with increasing distance from the crater center for larger primary craters than for smaller craters. On this basis, we expect secondary craters to be rather evenly distributed across our count areas. Since circular-shaped field secondaries in particular cannot always be completely removed from CSFD measurements, we performed additional randomness analyses (Michael et al., 2012; Figure 2) to further evaluate and minimize secondary cratering effects on our CSFDs.

While the use of very young reference surfaces minimizes the possibility that field secondary craters may significantly contaminate the count areas, self-secondary craters are a relatively greater concern especially for the smallest crater bins. This means that the selection of count areas is especially important for eliminating potential areas with concentrations of self-secondary craters. For example, the count areas from Plescia and Robinson (2019) with the highest number of craters at Giordano Bruno correspond to areas directly next to the rim or more than two crater diameters away on distal ejecta/rays. In contrast, we selected our count areas on flat areas within the continuous ejecta not far from the rim. Thus, we attempted to minimize the influence of self-secondary craters as much as possible.

However, a direct comparison with other authors is only possible to a limited extent since they investigated a different crater diameter range. H. J. Moore et al. (1980) found a shallower slope at North Ray, which was determined in the diameter range of 10–50 m; South Ray shows a shallower slope between 7 and 15 m in H. J. Moore et al. (1980); however, no count areas are shown.

4.4. Impactor Population

Ideally, the CSFD reflects the size frequency-distribution of impactors hitting the lunar surface (Baldwin, 1964; Neukum, 1983; Öpik, 1960). Several studies demonstrated that the impactor flux of the last 3 Ga was stable (e.g., Bottke et al., 2005; Guinness & Arvidson, 1977; Hiesinger et al., 2012; Neukum, 1983; Neukum et al., 2001; Stöffler et al., 2006; Xie & Xiao, 2023), although variations seem to be possible (e.g., Fassett et al., 2012; Marchi et al., 2009; McEwen et al., 1997). Since we investigate young Copernican-aged craters with a maximum age of 50 Ma, investigations of the recent bolide flux are relevant. H. J. Moore et al. (1980) measured impacts through passive seismic measurements on the lunar surface. They estimated a stable CSFD slope between −2.7 and −3.3 for craters between 1 and 100 m in the last 100 Ma. Alternately, Marchi et al. (2009) used a modeling approach and found evidence for a variable impactor flux in the last 500 Ma. The modeled slope of projectiles of near-Earth objects with sizes $<\sim$0.1 km is −2.6 (Marchi et al., 2009). Projectiles of ∼0.1 km correspond to a crater diameter of ∼1 km (Marchi et al., 2009). Xie et al. (2017) found a slope of about −3.2 for craters $\leq\sim$1 km, when considering the increase in crater diameters due to topographical degradation processes. Further details regarding the impactor population can be found in, for example, Fassett et al. (2018), Minton et al. (2015), Williams et al. (2022), and Ivanov (2006). The present-day crater-production rate was investigated by Speyerer et al. (2016), who studied recent impacts on the lunar surface with NAC images. Using multi-temporal NAC images, they quantified the recent production rate of craters on the Moon. They found that 33% more craters with diameters 10–43 m were formed on the lunar surface than proposed by Neukum (1983) and Neukum et al. (2001), and observed a steeper slope for the PF for craters ≥10 m.

We derived an averaged CSFD slope of −3.20, which equals 6.7% more craters than Neukum (1983) and Neukum et al. (2001), if we consider craters ≥10 m and between 10 and 20 m in our count areas (see Table 4). One possible explanation for this increase in craters ≥10 m and between 10 and 20 m is a variation in the number of projectiles hitting the lunar surface. Furthermore, slight changes in the CSFD slope might be as well a result of the Yarkovski Effect (a thermal radiation force, effecting the orbit of the impactor, Bottke et al., 2006; Hartmann et al., 1999) or break up events (Bottke et al., 2006).

However, not all areas on the lunar surface are considered to have the same probability of being hit by an impactor, yielding spatial variability in the distribution of impact craters. For instance, the works of Le Feuvre and Wieczorek (2008) and Gallant et al. (2009) implicate higher impact rates at the equator than at the poles. Gallant et al. (2009) used a numerical approach to calculate the latitudinal impactor distribution. As a result, they found that within ∼30° of the equator, the probability for an impact is 10% higher than within 30° of the poles. Giordano Bruno and Moore F are located at 37° and 35° latitudes, respectively. The latitudes of the North and South Rays are within 10° of the equator. Le Feuvre and Wieczorek (2008) modeled the impact probability on different terrestrial planets and concluded that the crater formation rate on the Moon between the poles and the equator is 0.90. In contrast, Werner and Medvedev (2010) found impact variations between <15% and 50% for rayed craters on the lunar surface with the highest number of craters at the poles. Morota and Furumoto (2003) investigated the impactor frequency depending on the longitude and found that the apex has a 1.5 times higher cratering rate than the antapex. In summary, this might indicate that the frequency of impacts is dependent on the location of the investigated areas. However, these regional changes are related to the entire cratering rate and should not be reflected in individual crater diameters and, therefore, do not affect the CSFD slope.

4.5. Evaluation of Count Areas and Statistical Errors

The used images have incidence angles between ∼54° and ∼78°, which is within the range of illuminations published by Antonenko et al. (2013), who found that the optimal incidence angles for crater detection is between ∼58° and ∼77°. Ostrach (2013) found the optimal incidence angle to be ∼80°. Our images show good contrast and a sufficient pixel resolution, allowing CSFD measurements to diameters down to 2.5 m, that is, five pixels to identify a crater.

Table 8
Combined Slopes and the Derived Uncertainties From the Algorithm of Clauset et al. (2009)

	Uncertainties of the CSFD slopes			
Count area	≤10 m	≥10 m	10–20 m	Full diameter range
Giordano Bruno 1	0.41	0.65	0.63	0.42
Giordano Bruno 2	0.21	0.36	0.31	0.17
Giordano Bruno 3	0.12	0.19	0.19	0.13
Combined Giordano Bruno	**0.11**	**0.15**	**0.16**	**0.11**
Moore F 1	0.05	0.15	0.16	0.05
Moore F 2	0.30	1.71	1.52	0.26
Moore F 3	0.05	0.21	0.19	0.05
Combined Moore F	**0.04**	**0.12**	**0.13**	**0.04**
North Ray 1	0.11	0.27	0.32	0.11
North Ray 2	0.18	0.36	0.34	0.20
North Ray 3	0.10	0.31	0.34	0.11
North Ray 4	0.11	0.25	0.26	0.12
Combined North Ray	**0.06**	**0.15**	**0.15**	**0.07**
South Ray 1	0.71			0.71
South Ray 2	0.72	0.58	0.58	0.70
South Ray 3	0.50			0.50
Combined South Ray	**0.30**	**0.41**	**0.41**	**0.26**

Note. The bold values represent the combined data.

We selected our areas to be representative of the ejecta deposit being free of obvious secondary craters and resurfacing processes. However, the count areas at Giordano Bruno 1 and Giordano Bruno 2 display a small kink in the CSFD, which might indicate a minor resurfacing. Neukum et al. (1975) determined the error of his PF to be <10% for crater diameters between 0.8 and 3 km and up to 25% for craters with a diameter range between 0.8 and 10 km. Since we focus on young and small craters that occur in large numbers, we had to select relatively small counting areas to limit the amount of work measuring craters. However, small counting areas often exhibit larger errors. For example, van der Bogert et al. (2015) compared CSFDs generated via Monte Carlo simulations of young lunar surfaces. They found a lower accuracy with an error of ∼10% for the determined AMAs in smaller area sizes. Pasckert et al. (2015) investigated relative ages and AMAs depending on the count area size at Tsiolkovsky crater, where they subdivided a 100 km^2 area into 25 areas of 4 km^2. They considered craters ≥10 m and found differences in the determined AMAs and observed reduced accuracy when using small count areas; however, all AMAs were within the error range of the large area size (10 km^2).

Ejecta blankets can have highly variable crater densities (Zanetti et al., 2017). The CSFD slope is relatively sensitive for CSFDs with sparsely populated crater bins, so that small changes in the CSFD result in a significantly different slope. Using the algorithm of Clauset et al. (2009) could counteract this by fitting the slope to the unbinned data. In general, one of the main challenges of our study was identifying suitable count areas, as the areas had to be young enough not to be in equilibrium, have a sufficiently thick ejecta blanket, be free of resurfacing and secondary craters, and also be representative of the crater of interest.

The commonly used PFs are valid only for crater diameters larger than 10 m and up to 300 km (Neukum, 1983; Neukum et al., 2001). For that range the

display of the $N(1)$ or $N(10)$, which describes the crater density for craters with ≤1 km or ≤10 km, respectively, are suitable. Our investigation, however, focusses on small crater diameters, mainly on craters ≤10 m, which would add an avoidable error if scaled to 1 km or 10 km reference diameter.

The $N(0.01)$ error (see Table 3) is calculated as

$$\text{Error } N(0.01) = \frac{N(0.01)}{\sqrt{n}}$$

with n as the number of all craters in the fit range.

We used the Matlab algorithm from Clauset et al. (2009) to calculate the slope uncertainties (Table 8).

4.6. Possible Expansion of Neukum's PFs

As mentioned, the commonly used PFs of Neukum (1983) and Neukum et al. (2001) are valid in a crater diameter range between 10 m and 300 km. Whereas the PF of Neukum (1983) continues relatively stable with a −3 slope toward crater diameters down to 1 m, the PF of Neukum et al. (2001), however, shows a very steep progression (Figure 5).

Our observations indicate that the −3 slope of Neukum (1983) continues for craters ≤10 m. The deviation in Figure 5 toward shallower slopes at 4 m might indicate a beginning roll-over as the image resolution limit is reached. The very steep, nearly asymptotic continuation of the PF of Neukum et al. (2001), starting at 7 m downwards, probably does not represent the true CSFD distribution, which proves the invalidation of the PF of Neukum et al. (2001) for craters ≤10 m.

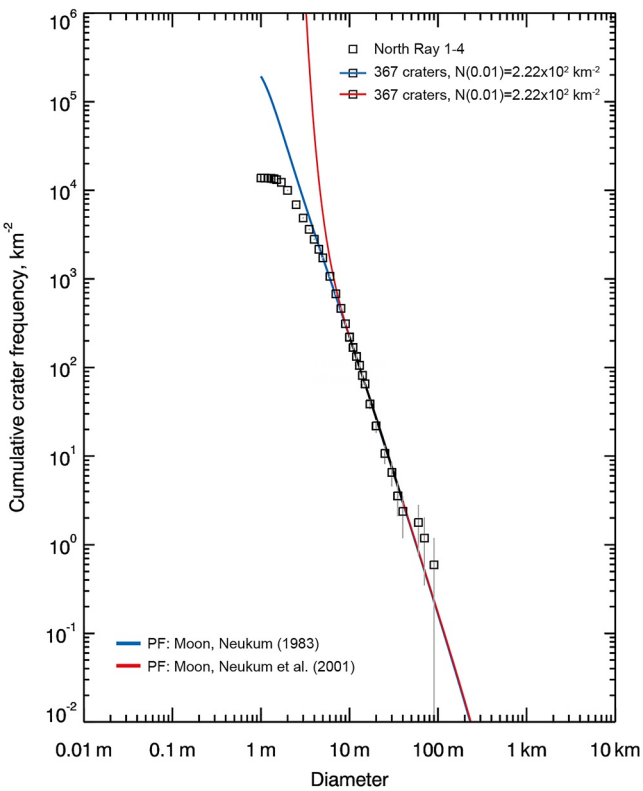

Figure 5. Behavior of the production functions of Neukum (1983, blue curve) and Neukum et al. (2001, red curve) for crater diameters down to 1 m at North Ray in the cumulative plot. The black overlap shows the fitted craters between 10 and 40 m.

5. Conclusion

We investigated the CSFD slopes of small craters on ejecta blankets at four Copernican-aged craters in the diameter ranges of ≤10, ≥10, 10 m–20 m, and across the full considered crater diameter range. The crater diameter range between 10 and 20 m allows us to compare the derived CSFD slopes directly with the PFs of Neukum (1983) and Neukum et al. (2001). We found CSFD slopes of −2.91 (≤10 m) and −3.20 (10–20 m) when combining all unaffected CSFD measurements. Due to the extraordinarily steep slope at Giordano Bruno, which is assumed to result from secondary cratering, we exclude this area for determining the CSFD slope for craters ≤10 m. These results indicate a slightly steeper CSFD slope for crater diameters between 10 and 20 m and ≥10 m compared to the −3 slope of Neukum (1983) and Neukum et al. (2001), as well as a CSFD slope of about −3 for craters ≤10 m, at least for young craters formed on ejecta blankets.

Small craters can be strongly affected by geological factors, including target properties (as different target materials, ejecta coverage from nearby craters, regolith coverage and regolith thickness, layering effects), crater degradation (diffusive crater degradation, mass wasting processes, seismic shaking), secondary cratering, and changes in the impactor population. We aimed to reduce these geological influences by detailed assessments of our count areas. Our investigation suggests that the observed changes in the CSFD slope likely reflect the craters in production rather than other geological processes.

Small craters are numerous and hence provide an opportunity to date smaller geological units and young features. Smaller craters (≤10 m) could provide valuable age information for locations where few secondaries are observed, equilibrium has not been reached, and only a limited area or small features are of interest (e.g., young lava flows, ejecta blankets, scarps).

Based on this investigation, we conclude that a PF can be developed for craters ≤10 m and that the PF of Neukum (1983) already provides a very plausible CSFD slope for craters ≤10 m formed on ejecta blankets, even though it is not designed to fit craters in that diameter range.

Data Availability Statement

The shapefiles of our count areas and the crater measurements are available in Oetting (2023). The LROC NAC images were obtained from the Planetary Data Systems (Robinson, 2011) and downloaded from https://ode.rsl.wustl.edu/moon/. NAC DTMs (Henriksen et al., 2017) were taken from https://wms.lroc.asu.edu/lroc/rdr_product_select. The Clementine ultraviolet-visible color ratio composite map of Lucey et al. (2000) was obtained from https://astrogeology.usgs.gov/search/map/Moon/Clementine/UVVIS/Lunar_Clementine_UVVIS_Warp_ClrRatio_Global_200m. To assess the potential for seismic activity from nearby lobate scarps, we used Quickmap (quickmap.lroc.asu.edu) lobate-scarp map (Nelson et al., 2014). The algorithm from Clauset et al. (2009) for calculating the CSFD slope and its uncertainties is available at https://aaronclauset.github.io/powerlaws/.

Acknowledgments
We thank the reviewers, Zongyu Yue and Mikhail Kreslavsky, for their constructive comments that greatly improved the manuscript. This project was funded by the Deutsche Forschungsgemeinschaft (DFG, German Research Foundation)—Project-ID 263649064—TRR 170. This is TRR Publication No. 196. CvdB is funded by the Deutsches Zentrum für Luft- und Raumfahrt (DLR, German Aerospace Center)—Project 50OW2001. Open Access funding enabled and organized by Projekt DEAL.

References

Anderson, J. A., Sides, S. C., Soltesz, D. L., Sucharski, T. L., & Becker, K. J. (2004). Modernization of the integrated software for imagers and spectrometers. In *Lunar and planetary science conference* (p. 2039).

Antonenko, I., Robbins, S. J., Gay, P. L., Lehan, C., & Moore, J. (2013). Effects of incidence angle on crater detection and the lunar ioschron system: Preliminary results from the CosmoQuest MoonMappers citizen science Project. In *44th annual lunar and planetary science conference* (No. (1719), p. 2705).

Arvidson, R., Crozaz, G., Drozd, R. J., Hohenberg, C. M., & Morgan, C. J. (1975). Cosmic ray exposure ages of features and events at the Apollo landing sites. *The Moon*, *13*(1), 259–276. https://doi.org/10.1007/BF00567518

Baldwin, R. B. (1964). Lunar crater counts. *The Astronomical Journal*, *69*, 377. https://doi.org/10.1086/109289

Baldwin, R. B. (1971). On the history of lunar impact cratering: The absolute time scale and the origin of planetesimals. *Icarus*, *14*(1), 36–52. https://doi.org/10.1016/0019-1035(71)90100-X

Basilevsky, A. T. (1976). On the rate of evolution of small lunar craters. In *Lunar and planetary science conference* (Vol. 7).

Basilevsky, A. T., & Head, J. W. (2012). Age of Giordano Bruno crater as deduced from the morphology of its secondaries at the Luna 24 landing site. *Planetary and Space Science*, *73*(1), 302–309. https://doi.org/10.1016/j.pss.2012.08.017

Basilevsky, A. T., Kozlova, N. A., Zavyalov, I. Y., Karachevtseva, I. P., & Kreslavsky, M. A. (2018). Morphometric studies of the Copernicus and Tycho secondary craters on the moon: Dependence of crater degradation rate on crater size. *Planetary and Space Science*, *162*, 31–40. https://doi.org/10.1016/j.pss.2017.06.001

Basilevsky, A. T., Kreslavsky, M. A., Karachevtseva, I. P., & Gusakova, E. N. (2014). Morphometry of small impact craters in the Lunokhod-1 and Lunokhod-2 study areas. *Planetary and Space Science*, *92*, 77–87. https://doi.org/10.1016/j.pss.2013.12.016

Behrmann, C., Crozaz, G., Drozd, R., Hohenberg, C., Ralston, C., Walker, R., & Yuhas, D. (1973). Cosmic-ray exposure history of North Ray and South Ray material. In *Lunar and planetary science conference proceedings* (Vol. 4, p. 1957).

Beyer, R. A., Alexandrov, O., & McMichael, S. (2018). NeoGeographyToolkit/StereoPipeline: NASA Ames stereo pipeline 2.6. 1 (version v2. 6.1).

Bottke, W. F., Jr., Durda, D. D., Nesvorný, D., Jedicke, R., Morbidelli, A., Vokrouhlický, D., & Levison, H. F. (2005). Linking the collisional history of the main asteroid belt to its dynamical excitation and depletion. *Icarus*, *179*(1), 63–94. https://doi.org/10.1016/j.icarus.2005.05.017

Bottke, W. F., Jr., Vokrouhlický, D., Rubincam, D. P., & Nesvorný, D. (2006). The Yarkovsky and YORP effects: Implications for asteroid dynamics. *Annual Review of Earth and Planetary Sciences*, *34*(1), 157–191. https://doi.org/10.1146/annurev.earth.34.031405.125154

Clauset, A., Shalizi, C. R., & Newman, M. E. (2009). Power-law distributions in empirical data. *SIAM Review*, *51*(4), 661–703. https://doi.org/10.1137/070710111

Crater Analysis Techniques Working Group. (1979). Standard techniques for presentation and analysis of crater size-frequency data. *Icarus*, *37*(2), 467–474. https://doi.org/10.1016/0019-1035(79)90009-5

Drozd, R. J., Hohenberg, C. M., Morgan, C. J., & Ralston, C. E. (1974). Cosmic-ray exposure history at the Apollo 16 and other lunar sites: Lunar surface dynamics. *Geochimica et Cosmochimica Acta*, *38*(10), 1625–1642. https://doi.org/10.1016/0016-7037(74)90178-1

Dundas, C. M., & McEwen, A. S. (2007). Rays and secondary craters of Tycho. *Icarus*, *186*(1), 31–40. https://doi.org/10.1016/j.icarus.2006.08.011

Fassett, C. I., Head, J. W., Kadish, S. J., Mazarico, E., Neumann, G. A., Smith, D. E., & Zuber, M. T. (2012). Lunar impact basins: Stratigraphy, sequence and ages from superposed impact crater populations measured from Lunar Orbiter Laser Altimeter (LOLA) data. *Journal of Geophysical Research*, *117*(E12), E00H06. https://doi.org/10.1029/2011JE003951

Fassett, C. I., Minton, D. A., Thomson, B. J., Hirabayashi, M., & Watters, W. A. (2018). Re-analysis of observations of crater degradation on the lunar maria accounting for anomalous diffusion. In *49th annual lunar and planetary science conference* (No. (2083), p. 1502).

Fassett, C. I., & Thomson, B. J. (2014). Crater degradation on the lunar maria: Topographic diffusion and the rate of erosion on the Moon. *Journal of Geophysical Research: Planets*, *119*(10), 2255–2271. https://doi.org/10.1002/2014JE004698

Gallant, J., Gladman, B., & Ćuk, M. (2009). Current bombardment of the Earth–Moon system: Emphasis on cratering asymmetries. *Icarus*, *202*(2), 371–382. https://doi.org/10.1016/j.icarus.2009.03.025

Gault, D. E. (1970). Saturation and equilibrium conditions for impact cratering on the lunar surface: Criteria and implications. *Radio Science*, *5*(2), 273–291. https://doi.org/10.1029/RS005i002p00273

Guinness, E. A., & Arvidson, R. E. (1977). On the constancy of the lunar cratering flux over the past 3.3 billion yr. In *Lunar and planetary science conference proceedings* (Vol. 8, pp. 3475–3494).

Hartmann, W. K. (1999). Martian cratering VI: Crater count isochrons and evidence for recent volcanism from Mars Global Surveyor. *Meteoritics & Planetary Sciences*, *34*(2), 167–177. https://doi.org/10.1111/j.1945-5100.1999.tb01743.x

Hartmann, W. K. (2005). Martian cratering 8: Isochron refinement and the chronology of Mars. *Icarus*, *174*(2), 294–320. https://doi.org/10.1016/j.icarus.2004.11.023

Hartmann, W. K., Farinella, P., Vokrouhlický, D., Weidenschilling, S. J., Morbidelli, A., Marzari, F., et al. (1999). Reviewing the Yarkovsky effect: New light on the delivery of stone and iron meteorites from the asteroid belt. *Meteoritics & Planetary Sciences*, *34*(S4), A161–A167. https://doi.org/10.1111/j.1945-5100.1999.tb01761.x

Hartmann, W. K., & Neukum, G. (2001). Cratering chronology and the evolution of Mars. In *Chronology and evolution of Mars: Proceedings of an ISSI workshop* (pp. 165–194). Springer Netherlands. https://doi.org/10.1007/978-94-017-1035-0_6

Hartmann, W. K., Strom, R. G., Weidenschilling, S. J., Blasius, K. R., Woronow, A., Dence, M. R., et al. (1981). Chronology of planetary volcanism by comparative studies of planetary craters. In *Basaltic volcanism on the terrestrial planets* (pp. 1050–1127). Pergamon.

Haruyama, J., Matsunaga, T., Ohtake, M., Morota, T., Honda, C., Yokota, Y., et al. (2008). Global lunar-surface mapping experiment using the Lunar Imager/Spectrometer on SELENE. *Earth Planets and Space*, *60*(4), 243–255. https://doi.org/10.1186/BF03352788

Henriksen, M. R., Manheim, M. R., Burns, K. N., Seymour, P., Speyerer, E. J., Deran, A., et al. (2017). Extracting accurate and precise topography from LROC narrow angle camera stereo observations. *Icarus*, *283*, 122–137. https://doi.org/10.1016/j.icarus.2016.05.012

Heyer, T., Hiesinger, H., Reiss, D., Erkeling, G., Bernhardt, H., Luesebrink, D., & Jaumann, R. (2018). The multi-temporal database of planetary image data (MUTED): A web-based tool for studying dynamic Mars. *Planetary and Space Science*, *159*, 56–65. https://doi.org/10.1016/j.pss.2018.04.015

Hiesinger, H., Jaumann, R., Neukum, G., & Head, J. W., III. (2000). Ages of mare basalts on the lunar nearside. *Journal of Geophysical Research*, *105*(E12), 29239–29275. https://doi.org/10.1029/2000JE001244

Hiesinger, H., Van der Bogert, C. H., Pasckert, J. H., Funcke, L., Giacomini, L., Ostrach, L. R., & Robinson, M. S. (2012). How old are young lunar craters? *Journal of Geophysical Research*, *117*(E12), E00H10. https://doi.org/10.1029/2011JE003935

Housen, K. R., & Holsapple, K. A. (2011). Ejecta from impact craters. *Icarus*, *211*(1), 856–875. https://doi.org/10.1016/j.icarus.2010.09.017

Ivanov, B. A. (2006). Earth/Moon impact rate comparison: Searching constraints for lunar secondary/primary cratering proportion. *Icarus*, *183*(2), 504–507. https://doi.org/10.1016/j.icarus.2006.04.004

Ivanov, B. A., & Hartmann, W. K. (2007). Exogenic dynamics, cratering and surface ages. Planets and Moons. *Treatise on Geophysics*, *10*, 207–242. https://doi.org/10.1016/B978-044452748-6.00158-9

Ivanov, B. A., Neukum, G., Bottke, W. F., & Hartmann, W. K. (2002). The comparison of size-frequency distributions of impact craters and asteroids and the planetary cratering rate. *Asteroids III*, *1*, 89–101.

Ivanov, B. A., Neukum, G., & Wagner, R. (2001). Size-frequency distributions of planetary impact craters and asteroids. In *Collisional processes in the solar system* (pp. 1–34). Springer. https://doi.org/10.1007/978-94-010-0712-2_1

Kneissl, T., van Gasselt, S., & Neukum, G. (2011). Map-projection-independent crater size-frequency determination in GIS environments—New software tool for ArcGIS. *Planetary and Space Science*, *59*(11–12), 1243–1254. https://doi.org/10.1016/j.pss.2010.03.015

König, B. (1977). *Investigations of primary and secondary impact structures on the Moon and laboratory experiments to study the ejecta of secondary particles* (No. NASA-TM-75023). NASA.

Krüger, T., Kenkmann, T., & Hergarten, S. (2017). Structural uplift and ejecta thickness of lunar mare craters: New insights into the formation of complex crater rims. *Meteoritics & Planetary Sciences*, *52*(10), 2220–2240. https://doi.org/10.1111/maps.12925

Le Feuvre, M., & Wieczorek, M. A. (2008). Nonuniform cratering of the terrestrial planets. *Icarus*, *197*(1), 291–306. https://doi.org/10.1016/j.icarus.2008.04.011

Lucey, P. G., Blewett, D. T., Taylor, G. J., & Hawke, B. R. (2000). Imaging of lunar surface maturity. *Journal of Geophysical Research*, *105*(E8), 20377–20386. https://doi.org/10.1029/1999JE001110

Mahanti, P., Robinson, M. S., Thompson, T. J., & Henriksen, M. R. (2018). Small lunar craters at the Apollo 16 and 17 landing sites-morphology and degradation. *Icarus*, *299*, 475–501. https://doi.org/10.1016/j.icarus.2017.08.018

Marchi, S., Mottola, S., Cremonese, G., Massironi, M., & Martellato, E. (2009). A new chronology for the Moon and Mercury. *The Astronomical Journal*, *137*(6), 4936–4948. https://doi.org/10.1088/0004-6256/137/6/4936

Marti, K., Lightner, B. D., & Osborn, T. W. (1973). Krypton and xenon in some lunar samples and the age of North Ray Crater. In *Lunar and planetary science conference proceedings* (Vol. 4, p. 2037).

McEwen, A. S., & Bierhaus, E. B. (2006). The importance of secondary cratering to age constraints on planetary surfaces. *Annual Review of Earth and Planetary Sciences*, *34*(1), 535–567. https://doi.org/10.1146/annurev.earth.34.031405.125018

McEwen, A. S., Moore, J. M., & Shoemaker, E. M. (1997). The Phanerozoic impact cratering rate: Evidence from the farside of the Moon. *Journal of Geophysical Research*, *102*(E4), 9231–9242. https://doi.org/10.1029/97JE00114

Melosh, H. J. (1989). *Impact cratering: A geologic process*. Oxford University Press, Clarendon Press.

Michael, G. G., Kneissl, T., & Neesemann, A. (2016). Planetary surface dating from crater size-frequency distribution measurements: Poisson timing analysis. *Icarus*, *277*, 279–285. https://doi.org/10.1016/j.icarus.2016.05.019

Michael, G. G., Platz, T., Kneissl, T., & Schmedemann, N. (2012). Planetary surface dating from crater size–frequency distribution measurements: Spatial randomness and clustering. *Icarus*, *218*(1), 169–177. https://doi.org/10.1016/j.icarus.2011.11.033

Minton, D. A., Fassett, C. I., Hirabayashi, M., Howl, B. A., & Richardson, J. E. (2019). The equilibrium size-frequency distribution of small craters reveals the effects of distal ejecta on lunar landscape morphology. *Icarus*, *326*, 63–87. https://doi.org/10.1016/j.icarus.2019.02.021

Minton, D. A., Richardson, J. E., & Fassett, C. I. (2015). Re-examining the main asteroid belt as the primary source of ancient lunar craters. *Icarus*, *247*, 172–190. https://doi.org/10.1016/j.icarus.2014.10.018

Moore, H. J., Boyce, J. M., & Hahn, D. A. (1980). Small impact craters in the lunar regolith—Their morphologies, relative ages, and rates of formation. *The Moon and the Planets*, *23*(2), 231–252. https://doi.org/10.1007/BF00899820

Moore, J. M., & McEwen, A. S. (1996). The abundance of large, Copernican-age craters on the Moon. In *Lunar and planetary science conference* (Vol. 27).

Morota, T., & Furumoto, M. (2003). Asymmetrical distribution of rayed craters on the Moon. *Earth and Planetary Science Letters*, *206*(3–4), 315–323. https://doi.org/10.1016/S0012-821X(02)01111-1

Morota, T., Haruyama, J., Miyamoto, H., Honda, C., Ohtake, M., Yokota, Y., et al. (2009). Formation age of the lunar crater Giordano Bruno. *Meteoritics & Planetary Sciences*, *44*(8), 1115–1120. https://doi.org/10.1111/j.1945-5100.2009.tb01211.x

Nakamura, Y., Latham, G. V., Dorman, H. J., Ibrahim, A. B., Koyama, J., & Horvath, P. (1979). Shallow moonquakes-depth, distribution and implications as to the present state of the lunar interior. In *Lunar and planetary science conference proceedings* (Vol. 10, pp. 2299–2309).

Nelson, D. M., Koeber, S. D., Daud, K., Robinson, M. S., Watters, T. R., Banks, M. E., & Williams, N. R. (2014). Mapping lunar maria extents and lobate scarps using LROC image products. In *Lunar and planetary science conference* (Vol. 45, p. 2861).

Neukum, G. (1983). *Meteoritenbombardement und Datierung planetarer Oberflächen, Habilitation dissertation for faculty membership* (p. 186). Ludwig-Maximilians-University.

Neukum, G., & Ivanov, B. A. (1994). Crater size distributions and impact probabilities on earth from lunar, terrestrial-planet, and asteroid cratering data. *Hazards due to Comets and Asteroids*, 359–416. https://doi.org/10.2307/j.ctv23khmpv.18

Neukum, G., Ivanov, B. A., & Hartmann, W. K. (2001). Cratering records in the inner solar system in relation to the lunar reference system. *Space Science Reviews*, *96*, 55–86. https://doi.org/10.1007/978-94-017-1035-0_3

Neukum, G., König, B., & Arkani-Hamed, J. (1975). A study of lunar impact crater size-distributions. *The Moon*, *12*(2), 201–229. https://doi.org/10.1007/BF00577878

Oberbeck, V. R., & Morrison, R. H. (1973). On the formation of the lunar herringbone pattern. In *Lunar and planetary science conference proceedings* (Vol. 4, p. 107).

Oetting, A. (2023). Shapefiles for count areas at Giordano Bruno, Moore F, North Ray, and South Ray [Dataset]. Dataverse, TRR170-DB. https://doi.org/10.35003/V9AFAZ

Öpik, E. J. (1960). The lunar surface as an impact counter. *Monthly Notices of the Royal Astronomical Society*, *120*(5), 404–411. https://doi.org/10.1093/mnras/120.5.404

Ostrach, L. R. (2013). Impact-related processes on Mercury and the Moon. PhD Thesis.

Pasckert, J. H., Hiesinger, H., & van der Bogert, C. H. (2015). Small-scale lunar farside volcanism. *Icarus*, *257*, 336–354. https://doi.org/10.1016/j.icarus.2015.04.040

Plescia, J. B., & Robinson, M. S. (2011). New constraints on the absolute lunar cratering chronology. In *42nd annual lunar and planetary science conference* (No. (1608), p. 1839).

Plescia, J. B., & Robinson, M. S. (2019). Giordano Bruno: Small crater populations—Implications for self-secondary cratering. *Icarus*, *321*, 974–993. https://doi.org/10.1016/j.icarus.2018.09.029

Plescia, J. B., Robinson, M. S., & Paige, D. A. (2010). Giordano Bruno: The young and the restless. In *41st annual lunar and planetary science conference* (No. (1533), p. 2038).

Richardson, J. E., Melosh, H. J., & Greenberg, R. (2004). Impact-induced seismic activity on asteroid 433 Eros: A surface modification process. *Science*, *306*(5701), 1526–1529. https://doi.org/10.1126/science.1104731

Richardson, J. E., Jr., Melosh, H. J., Greenberg, R. J., & O'Brien, D. P. (2005). The global effects of impact-induced seismic activity on fractured asteroid surface morphology. *Icarus*, *179*(2), 325–349. https://doi.org/10.1016/j.icarus.2005.07.005

Robbins, S. J. (2014). New crater calibrations for the lunar crater-age chronology. *Earth and Planetary Science Letters*, *403*, 188–198. https://doi.org/10.1016/j.epsl.2014.06.038

Robbins, S. J., Riggs, J. D., Weaver, B. P., Bierhaus, E. B., Chapman, C. R., Kirchoff, M. R., et al. (2018). Revised recommended methods for analyzing crater size-frequency distributions. *Meteoritics & Planetary Sciences*, *53*(4), 891–931. https://doi.org/10.1111/maps.12990

Robinson, M. S. (2011). LRO MOON LROC 5 RDR V1.0 [Dataset]. NASA Planetary Data System. https://doi.org/10.17189/1520341

Robinson, M. S., Brylow, S. M., Tschimmel, M., Humm, D., Lawrence, S. J., Thomas, P. C., et al. (2010). Lunar reconnaissance orbiter camera (LROC) instrument overview. *Space Science Reviews*, *150*(1), 81–124. https://doi.org/10.1007/s11214-010-9634-2

Ross, H. P. (1968). A simplified mathematical model for lunar crater erosion. *Journal of Geophysical Research*, *73*(4), 1343–1354. https://doi.org/10.1029/JB073i004p01343

Schultz, P., & Spencer, J. (1979). Effects of substrate strength on crater statistics: Implications for surface ages and gravity scaling. In *Lunar and planetary science conference* (Vol. 10, pp. 1081–1083).

Senthil Kumar, P., Keerthi, V., Senthil Kumar, A., Mustard, J., Gopala Krishna, B., Ostrach, L. R., et al. (2013). Gullies and landslides on the Moon: Evidence for dry-granular flows. *Journal of Geophysical Research: Planets*, *118*(2), 206–223. https://doi.org/10.1002/jgre.20043

Shoemaker, E. M. (1962). Interpretation of lunar craters. *Physics and Astronomy of the Moon*, 283–359.

Shoemaker, E. M. (1965). Preliminary analysis of the fine structure of the lunar surface in Mare Cognitum. *The Nature of the Lunar Surface*, (65), 23.

Shoemaker, E. M., Hait, M. H., Swann, G. A., Schleicher, D. L., Dahlem, D. H., Schaber, G. G., & Sutton, R. L. (1970). Lunar regolith at tranquillity base. *Science*, *167*(3918), 452–455. https://doi.org/10.1126/science.167.3918.452

Singer, K. N., Jolliff, B. L., & McKinnon, W. B. (2020). Lunar secondary craters and estimated ejecta block sizes reveal a scale-dependent fragmentation trend. *Journal of Geophysical Research: Planets*, *125*(8), e2019JE006313. https://doi.org/10.1029/2019JE006313

Soderblom, L. A., & Lebofsky, L. A. (1972). Technique for rapid determination of relative ages of lunar areas from orbital photography. *Journal of Geophysical Research*, *77*(2), 279–296. https://doi.org/10.1029/JB077i002p00279

Speyerer, E. J., Povilaitis, R. Z., Robinson, M. S., Thomas, P. C., & Wagner, R. V. (2016). Quantifying crater production and regolith overturn on the Moon with temporal imaging. *Nature*, *538*(7624), 215–218. https://doi.org/10.1038/nature19829

Stöffler, D., & Ryder, G. (2001). Stratigraphy and isotope ages of lunar geologic units: Chronological standard for the inner solar system. *Chronology and evolution of Mars*, *96*(1/4), 9–54. https://doi.org/10.1023/A:1011937020193

Stöffler, D., Ryder, G., Ivanov, B. A., Artemieva, N. A., Cintala, M. J., & Grieve, R. A. (2006). Cratering history and lunar chronology. *Reviews in Mineralogy and Geochemistry*, *60*(1), 519–596. https://doi.org/10.2138/rmg.2006.60.05

Titley, S. R. (1966). Seismic energy as an agent of morphologic modification on the Moon. In *Astrogeologic studies, annual progress report Part A lunar and planetary investigations* (pp. 87–103). U. S. Geological Survey. NASA-CR-8664.

Trask, N. J. (1966). *Size and spatial distribution of craters estimated from the ranger photographs in ranger VIII and IX, Part II, experimenters' analyses and interpretations*. Technical Report 32-800 (pp. 252–264). California Institute of Technology, Jet Propulsion Laboratory.

Trask, N. J. (1971). *Geologic comparison of mare materials in the lunar equatorial belt, including Apollo 11 and Apollo 12 landing sites* (Vol. 750D, pp. 2645–2662). U.S. Geological Survey Professional Paper.

Van der Bogert, C. H., Clark, J. D., Hiesinger, H., Banks, M. E., Watters, T. R., & Robinson, M. S. (2018). How old are lunar lobate scarps? 1. Seismic resetting of crater size-frequency distributions. *Icarus*, *306*, 225–242. https://doi.org/10.1016/j.icarus.2018.01.019

Van der Bogert, C. H., Hiesinger, H., Dundas, C. M., Krüger, T., McEwen, A. S., Zanetti, M., & Robinson, M. S. (2017). Origin of discrepancies between crater size-frequency distributions of coeval lunar geologic units via target property contrasts. *Icarus*, *298*, 49–63. https://doi.org/10.1016/j.icarus.2016.11.040

Van der Bogert, C. H., Hiesinger, H., McEwen, A. S., Dundas, C., Bray, V., Robinson, M. S., et al. (2010). Discrepancies between crater size-frequency distributions on ejecta and impact melt pools at lunar craters: An effect of differing target properties? In *41st annual lunar and planetary science conference* (No. (1533), p. 2165).

Van der Bogert, C. H., Michael, G., Kneissl, T., Hiesinger, H., & Pasckert, J. H. (2015). Development of guidelines for recommended lunar CSFD count area sizes via analysis of random CSFDs. *Issues in Crater Studies and the Dating of Planetary Surfaces*, *1841*, 9023.

Watters, T. R., Robinson, M. S., Collins, G. C., Banks, M. E., Daud, K., Williams, N. R., & Selvans, M. M. (2015). Global thrust faulting on the Moon and the influence of tidal stresses. *Geology*, *43*(10), 851–854. https://doi.org/10.1130/G37120.1

Watters, T. R., Weber, R. C., Collins, G. C., Howley, I. J., Schmerr, N. C., & Johnson, C. L. (2019). Shallow seismic activity and young thrust faults on the Moon. *Nature Geoscience*, *12*(6), 411–417. https://doi.org/10.1038/s41561-019-0362-2

Weber, R. C., Bills, B. G., & Johnson, C. L. (2009). Constraints on deep moonquake focal mechanisms through analyses of tidal stress. *Journal of Geophysical Research*, *114*(E5), E05001. https://doi.org/10.1029/2008JE003286

Werner, S. C., & Ivanov, B. A. (2015). Exogenic dynamics, cratering, and surface ages. *Treatise on Geophysics*, 327–365. https://doi.org/10.1016/B978-0-444-53802-4.00170-6

Werner, S. C., & Medvedev, S. (2010). The lunar rayed-crater population—Characteristics of the spatial distribution and ray retention. *Earth and Planetary Science Letters*, *295*(1–2), 147–158. https://doi.org/10.1016/j.epsl.2010.03.036

Williams, J. P., Pathare, A. V., Costello, E. S., Gallinger, C. L., Hayne, P. O., Ghent, R. R., et al. (2022). The effects of terrain properties upon the small crater population distribution at Giordano Bruno: Implications for lunar chronology. *Journal of Geophysical Research: Planets*, *127*(5), e2021JE007131. https://doi.org/10.1029/2021JE007131

Wünnemann, K., Marchi, S., Nowka, D., & Michel, P. (2012). The effect of target properties on impact crater scaling and the lunar crater chronology. In *43rd annual lunar and planetary science conference* (No. (1659), p. 1805).

Wünnemann, K., Nowka, D., Collins, G. S., Elbeshausen, D., & Bierhaus, M. (2011). Scaling of impact crater formation on planetary surfaces—Insights from numerical modeling. In *Proceedings of the 11th hypervelocity impact symposium* (Vol. 20, pp. 1–16). Fraunhofer Verlag.

Xiao, Z., & Strom, R. G. (2012). Problems determining relative and absolute ages using the small crater population. *Icarus*, *220*(1), 254–267. https://doi.org/10.1016/j.icarus.2012.05.012

Xiao, Z., Zeng, Z., Ding, N., & Molaro, J. (2013). Mass wasting features on the Moon–how active is the lunar surface? *Earth and Planetary Science Letters*, *376*, 1–11. https://doi.org/10.1016/j.epsl.2013.06.015

Xie, M., & Xiao, Z. (2023). A new chronology from debiased crater densities: Implications for the origin and evolution of lunar impactors. *Earth and Planetary Science Letters*, *602*, 117963. https://doi.org/10.1016/j.epsl.2022.117963

Xie, M., Xiao, Z., & Xu, A. (2019). Time-dependent production functions of lunar simple craters on layered targets with consideration of topographic degradation. *Geophysical Research Letters*, *46*(20), 10987–10996. https://doi.org/10.1029/2019GL084097

Xie, M., Zhu, M. H., Xiao, Z., Wu, Y., & Xu, A. (2017). Effect of topography degradation on crater size-frequency distributions: Implications for populations of small craters and age dating. *Geophysical Research Letters*, *44*(20), 10–171. https://doi.org/10.1002/2017GL075298

Zanetti, M., Stadermann, A., Jolliff, B., Hiesinger, H., Van der Bogert, C. H., & Plescia, J. (2017). Evidence for self-secondary cratering of Copernican-age continuous ejecta deposits on the Moon. *Icarus*, *298*, 64–77. https://doi.org/10.1016/j.icarus.2017.01.030